Received: 10 April 2021 | Revised: 10 September 2021 | Accepted: 18 October 2021

DOI: 10.1002/eqe.3569

RESEARCH ARTICLE

WILEY

Effects of vertical ground motions on the dynamic response of URM structures: Comparative shake-table tests

Stylianos Kallioras[1,2] | **Francesco Graziotti**[1,2] | **Andrea Penna**[1,2] | **Guido Magenes**[1,2]

[1] Department of Civil Engineering and Architecture (DICAr), University of Pavia, Pavia, Italy

[2] European Centre for Training and Research in Earthquake Engineering (EUCENTRE), Pavia, Italy

Correspondence
Francesco Graziotti, DICAr University of Pavia & EUCENTRE, Via Adolfo Ferrata 1-3, 27100 Pavia (PV), Italy.
Email: francesco.graziotti@unipv.it

Funding information
Italian Department of Civil Protection; Nederlandse Aardolie Maatschappij BV

Abstract

This paper discusses the results of an experimental study aimed at evaluating the influence of the vertical ground motion component on the seismic performance of unreinforced brick-masonry buildings. The research was motivated by post-earthquake observations of significant structural damage in the vicinity of the fault, where horizontal and vertical ground motions are often strong and synchronized. Vertical accelerations can fluctuate gravity loads, which control the in-plane lateral load capacity of masonry piers and affect the out-of-plane overturning stability of thin walls. Such phenomena seem not to be sufficiently explained in existing literature, while experimental evidence is undoubtedly missing. Here, the damage potential of vertical accelerations was investigated through a series of multidirectional shake-table tests on full-scale structures under simulated near-source ground motions of increasing intensity. The experiments comprised three nominally identical building specimens subjected to the principal horizontal component alone, the horizontal component combined with the vertical one, and the full three-component ground motion. The buildings included structural/nonstructural elements (e.g., gables, chimneys, and parapets) sensitive to gravity load variations due to their low axial loads. Two different sets of three-component earthquake records were employed to assess the effects of both tectonic and induced seismicity scenarios. Overall, the vertical earthquake motion did not cause appreciable differences in the behavior of the buildings. Any influence on the strength and peak response of structural/nonstructural walls was marginal and non-systematic. Data and observations from these experiments add substantially to our understanding of the vertical acceleration effects on masonry structures.

KEYWORDS
multidirectional seismic input, near-fault ground motion, rocking response, shake-table test, structural/nonstructural URM damage, vertical acceleration

1 | INTRODUCTION

The vertical component of ground motions has fueled a long debate about its significance in the seismic design and assessment of structures.[1] For many years, conventional wisdom holds that vertical accelerations may affect only horizontal cantilevers, long-span structural members, base-isolation devices, or nonstructural elements. However, as researchers worldwide have not reached a consensus about the importance of vertical earthquake motions, appropriate methods for incorporating their effects into structural analysis procedures are somehow missing. Consequently, vertical ground accelerations are generally overlooked or inadequately considered in practice for ordinary buildings.

One of the pioneer studies highlighting the importance of considering vertical accelerations in the structural design was conducted by Papazoglou and Elnashai.[2] Their seminal paper of 1996 collated field observations and analysis results illustrating the possible damaging effects of strong vertical ground motions on reinforced concrete (RC) structures. In two follow-up works, Elnashai et al. contradicted arguments suggesting that the vertical component can be disregarded on the basis of low peak ground acceleration and proposed shapes for vertical design spectra based on the observation that, in the near-field area, vertical short-period spectral ordinates often exceed the horizontal ones. The same researchers developed simple procedures for including vertical seismic actions in structural analyses but admitted that further improvements were still required.[3,4]

Seismic design codes have adopted approaches of varying complexity to deal with this aspect of earthquake effects. A simple rule was first proposed by Newmark et al.,[5] who suggested that the vertical design spectrum shall be taken as two-thirds of the horizontal spectrum, implying that the vertical-to-horizontal (V/H) spectral ratio is constant over all periods. In the years that followed, this approach received criticism for underestimating vertical motion effects at short periods, especially at sites near the fault. Since then, several studies have demonstrated that the V/H ratio strongly depends on the natural period, source-to-site distance, and local site conditions (in refs.[6,7] and references reported therein). Modern seismic design codes in the US and Europe have recognized such findings and introduced independent formulations for horizontal and vertical design spectra.[8–10] Nonetheless, the controversy over the significance of vertical motions to the structural response remains unresolved.

The past decade has seen a renewed interest in understanding the role of vertical earthquake motion on the severe structural damage observed at sites near the fault.[11–13] Recently, Liberatore et al.[14] referred to the evidence of vertical ground motions from InSAR data to explain the extensive damage to unreinforced masonry (URM) buildings in the area affected by the 2016 Amatrice-Norcia earthquakes in Central Italy. The same researchers demonstrated the adverse effects of vertical accelerations on low-shear-resistance masonry structures by referring to numerical analysis results. Other investigators have also drawn attention to the potential negative impact of axial load fluctuations on the seismic demand-to-capacity relationship in old URM buildings,[15,16] as well as on precast RC structures.[17] However, these findings rely on numerical simulations only, while experimental evidence is still lacking. Only recently, Tsiavos et al.[18] observed through experimentation that the dynamic response of a seismically isolated URM structure was not particularly affected by the presence of high-frequency vertical accelerations, suggesting that further research should be conducted before deriving firm conclusions.

In the present study, a series of full-scale shake-table tests were carried out to investigate the influence of vertical ground motions on the seismic behavior of URM buildings and provide an experimental reference for numerical modeling. Incremental dynamic tests were performed on three identical structures at the multiaxial shaking table of EUCENTRE in Pavia, Italy. The first specimen, labeled EUC-BUILD-8.1, was subjected to the principal horizontal motion only; the second specimen, EUC-BUILD-8.2, to the horizontal motion combined with the vertical one; and the third one, EUC-BUILD-8.3, was subjected to all three ground motion components simultaneously. The prototype was a generic, single-story building made of solid clay bricks, with a flexible floor diaphragm and wide openings at all façades. It included a gable wall, chimneys, and parapets, which appear to be more sensitive to gravity load variations due to low axial loads. Ground shaking of increasing intensity was applied to each building up to near-collapse conditions, using two sets of real earthquake accelerograms. The second was a tectonic ground motion specifically selected to maximize the possible effects of the combined horizontal and vertical shaking. All specimens were densely instrumented with sensors that recorded the three-dimensional response of various structural elements.

This paper begins with a brief overview of the geometric and mechanical characteristics of the test buildings. Next, it presents the selected input ground motions, focusing on the relative intensity and synchronization of the vertical and horizontal components. Subsequent sections discuss the major observations from the tests, including damage evolution, motion amplification effects, hysteretic responses, and peak displacement demands. Finally, the influence of vertical

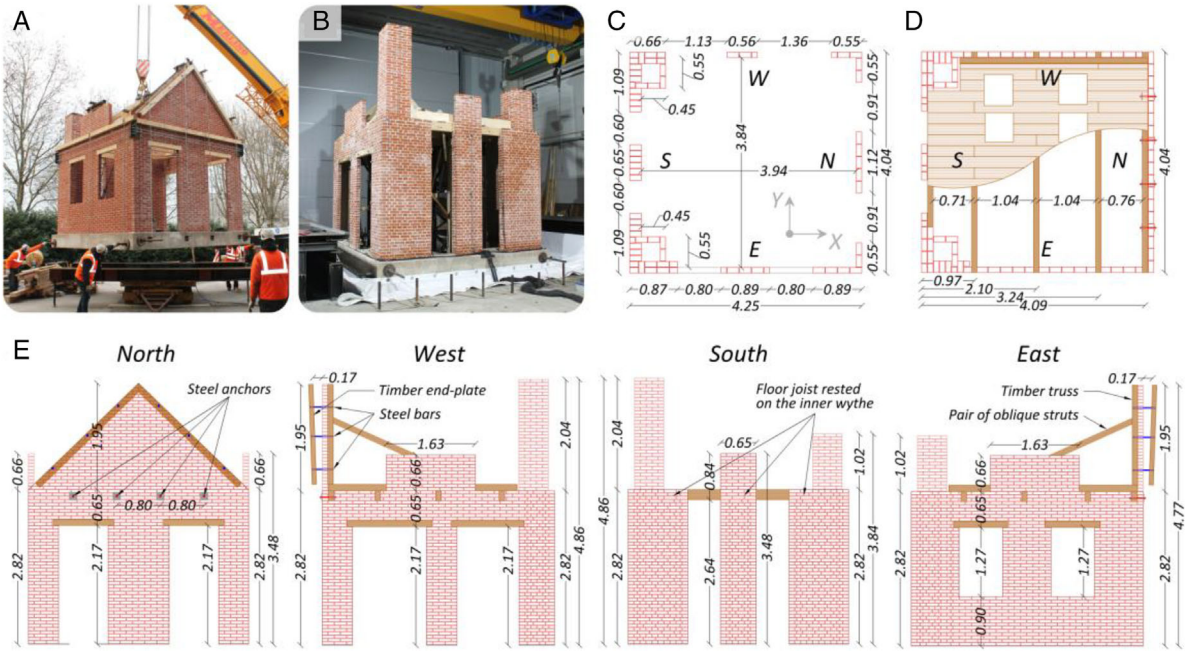

FIGURE 1 Full-scale prototype building: (A) North-East view of a specimen during transportation; (B) South-West view of a specimen on the shake table; (C) ground-floor plan; (D) floor framing plan; (E) elevation views (units of m). In blue are the steel bars holding the timber end-plate of the gable; in red are the four wall-to-diaphragm steel connectors

accelerations is assessed by analyzing global and local response mechanisms separately. Overall, the article provides experimental results that might help understand the vertical ground motion effects on URM structures.

2 | SPECIMENS OVERVIEW

2.1 | Geometry and construction details

The building specimens were identical in geometry and construction details. The prototype was a generic single-story structure characterized by a 2.82-m floor height (measured to the top of the floorboards). All specimens featured a 1.95-m-high gable wall, two chimneys of different slenderness, and three parapets extending over the floor (Figure 1A,B). The walls were built in a rectangular layout (Figure 1C,D): the overall footprint dimensions were 4.25 m in the longitudinal direction (i.e., South-North) and 4.04 m in the transverse one (i.e., East-West). Throughout this paper, letters X, Y, and Z will refer to the longitudinal, transverse, and vertical building directions, respectively.

The load-bearing structural system consisted of URM walls supported by an RC foundation. The walls were constructed employing $215 \times 100 \times 50$ mm^3 solid clay bricks and 10-mm-thick, fully mortared head- and bed-joints made of hydraulic lime mortar (NHL 3.5 according to Ref.[19]). The mortar was prepared by mixing 25 kg of powder with 4.3 kg of water. Extra sand was added to the mortar mix in ratio 1:4 to slightly reduce the original strength of the mortar, targeting moderate strength values typical of existing URM buildings. Three out of the four perimeter walls, that is, the North, East, and West walls, consisted of a single 100-mm-wide leaf built with the standard stretcher bond. The South façade was made of a double, 215-mm-thick wythe, using the *Dutch cross* brickwork bond to facilitate interlocking with the chimneys (Figure 2A). Large asymmetric openings were present at all façades, resulting in varying wall areas in the two horizontal directions (Figure 1E). The intention was to magnify differential wall displacements and trigger different in-plane failure mechanisms for the piers under combined horizontal and vertical motions. Lintels were placed above all openings: they were 110-mm-deep timber beams, extending into the masonry 100 mm on each side of the openings for support (Figure 2B).

The floor system consisted of 300-mm-wide × 30-mm-thick timber floorboards nailed to five 100-mm-wide × 180-mm-deep timber joists, stretching continuously across the East-West direction (Figure 2C). The floorboard-to-joist connections were realized using two nails at each intersection, resulting in a flexible diaphragm. The joists were supported by the East, West, and South walls. At the North façade, four steel anchors were installed at the floor level (highlighted in red in

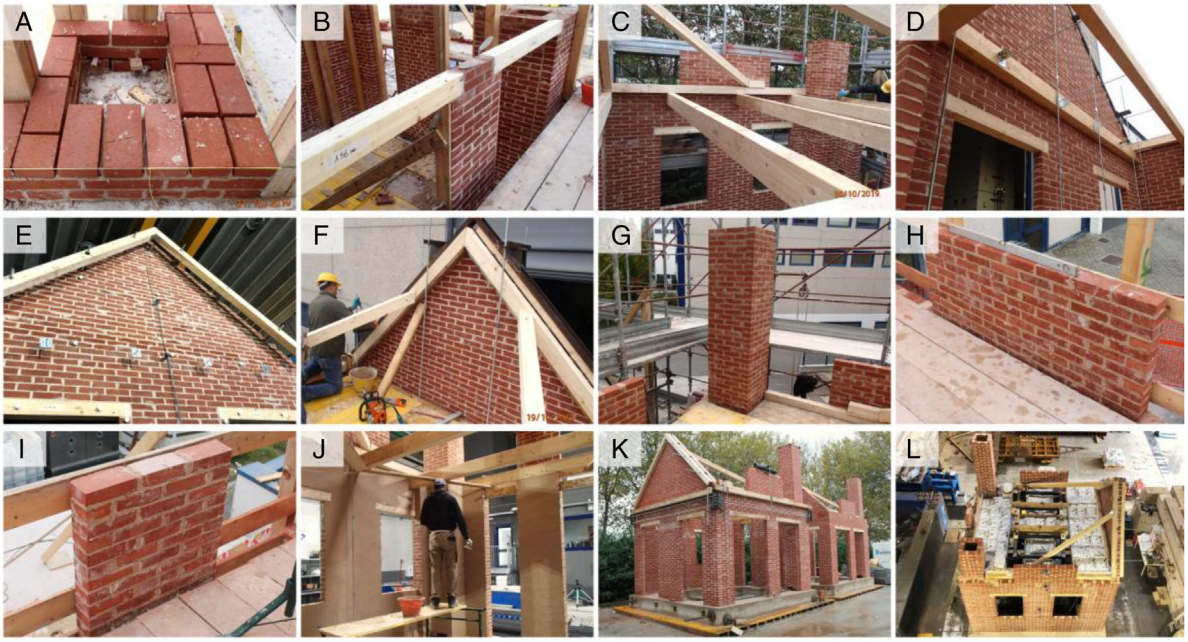

FIGURE 2 Construction details of the prototype building: (A) Dutch cross brickwork bond and interlocking between perimeter wall and chimney; (B) timber lintels above the openings; (C) floor joists during construction; (D) wall-to-diaphragm connections at North façade (initially deactivated); (E) end-plate preventing a collapse of the North gable (initially at a distance from the wall); (F) truss and struts at North gable; (G) slender chimney at South-West corner; (H) parapet wall at East façade; (I) parapet wall at South façade; (J) plastering the inner face of the masonry walls; (K) temporary strengthening measures for specimen transportation; (L) additional masses on the floor diaphragm

Figure 1D,E), restraining this wall against out-of-plane overturning. The anchors consisted of 5-mm-thick steel plates, held in place by 8-mm-diameter rods. They were provided at a spacing of 0.8 m at the gable-floor joints and were screwed on the interior side to the first joist from the North wall (Figure 2D,E). These devices were not connected to the timber floor framing initially but were placed with the possibility to be activated subsequently, in case of the early development of a local out-of-plane mechanism of the North façade.

A timber truss was placed back-to-back with the triangular gable wall, allowing only the one-side rocking response of the latter.[20] Struts were provided to support the truss rafters (at about two-thirds of the gable height) and transfer to the floor frame any loads caused by the impacts of the gable wall on the truss (Figure 2F). Rafters and struts were supported by timber lower plates screwed perpendicularly to the floor joists at the locations where the latter were recessed into the masonry (Figure 2C). A timber plate was installed outside the gable, forming an end-plate that prevented collapse due to the out-of-plane overturn of the wall (Figure 2E). Initially, the plate was suspended by the roof truss through six 20-mm-diameter steel bars (highlighted in blue in Figure 1D,E). It was placed at a distance from the wall that allowed relative displacements between gable tip and roof truss up to 170 mm, just a few millimeters over the relative displacement causing static instability of the gable (approximately equal to 150 mm).

The building specimens included two URM chimneys at the vertical edges of the South façade, with a 540-mm-wide square section and flue size of 340×340 mm^2. The chimney at the intersection with the West wall was moderately slender, extending 2.0 m above the floor diaphragm (Figure 2G), while the East chimney was squatter as it penetrated the floor for 1.0 m. Three 0.66-m-high parapets with varying lengths were built on top of the East, West, and South walls, as illustrated in Figure 2H,I. The interior of the buildings was coated with 3-mm-thin lime plaster to facilitate detecting cracks and assess nonstructural damage to the masonry walls during the post-test surveys (Figure 2J).

The construction works took place off the shake table to allow for the parallel construction of the specimens. The same batches of materials were used for all buildings to reduce the variability of their mechanical characteristics. The structures were built within about 40 days to moderate the effect of varying environmental conditions on the curing process and ultimate strength of mortar. Transportation onto the shake table was done after a maturation period of about a month following the construction. Overburden stress of approximately 0.10–0.15 MPa was applied on top of the perimeter walls, chimneys, parapets, and gable, to prevent the development of tensile stresses and consequent cracking of the masonry. Horizontal loads were also applied at the corners of each structure through a system of four L-shaped steel plates and

TABLE 1 Summary of masonry mechanical properties for the three test buildings

Material property (units)	EUC-BUILD-8.1		EUC-BUILD-8.2		EUC-BUILD-8.3	
	Avg.	C.o.V.	Avg.	C.o.V.	Avg.	C.o.V.
Density of masonry[a], ρ_m (kg/m^3)	1950	–	1950	–	1950	–
Brick standard compressive strength[a], f_b (MPa)	43.5	0.10	43.5	0.10	43.5	0.10
Brick flexural strength, f_{bt} (MPa)	N/A	N/A	N/A	N/A	N/A	N/A
Mortar compressive strength, f_c (MPa)	3.93	0.13	4.71	0.22	4.30	0.14
Mortar flexural strength, f_t (MPa)	1.14	0.24	1.37	0.24	1.36	0.21
Masonry compressive strength, f_m (MPa)	9.74	0.19	11.1	0.05	11.7	0.09
Masonry Young's modulus in compression[b], E_{m1} (MPa)	5320	0.28	7000	0.37	6690	0.28
Masonry flexural bond strength, f_w (MPa)	0.23	0.33	0.14	0.23	0.13	0.37
Masonry (bed-joint) cohesion, f_{v0} (MPa)	0.50	–	0.66	–	0.71	–
Masonry (bed-joint) initial shear-friction coefficient, μ (–)	0.80	–	0.71	–	0.81	–

N/A: not available data. Flexural-tensile strength estimates for this type of bricks are provided in Refs.[27,28].
[a]Properties ρ_m and f_b were estimated from samples taken equally from all three buildings.
[b]Property E_{m1} was defined as the slope of the secant line through 33% of f_m on the σ-ε curve.

post-tensioned threaded steel bars, providing average axial stress equal to 0.10 MPa to the spandrel beams. All façades were restrained against out-of-plane deflections by a timber ring beam extending along the perimeter (Figure 2K). Consequently, the buildings did not suffer damage during the lifting operation. The necessity to transport the buildings was one of the reasons they did not comprise a roof. Nevertheless, additional masses were provided on the floor diaphragm to simulate the gravity loads resulting from the self-weight of a hypothetical timber roof frame finished with clay tiles (Figure 2L).

2.2 | Structural and nonstructural masses

A critical aspect of the experiments was to supply evidence of the vertical acceleration effects on the resistance of URM walls under realistic loading conditions. Overall, the masonry walls had a mass of 11.3 t, estimated with a mean density of 1950 kg/m^3. The timber floor diaphragm and roof truss provided a mass of 0.3 t. An additional mass of 1.1 t was placed on the floor, using 44 bags of 25 kg mortar (Figure 2L), evenly distributed over the diaphragm to account for superimposed dead and live loads (equivalent to approximately 67 kg/m^2). Two extra loads were placed at the East and West floor borders, each equal to 0.45 t. These masses emulated part of the self-weight of the missing roof, which would have been transferred to the longitudinal walls through trusses supported on the East and West edges of the floor. Once transported on the shake table, the total mass of each building specimen was 13.6 t.

2.3 | Mechanical properties of materials

A series of tests were carried out to determine the mechanical properties of the clay-brick masonry. They comprised strength tests on mortar samples and clay units,[21,22] as well as compression tests on masonry wallettes,[23] bond wrench tests on couplets,[24] and direct-shear tests on triplets.[25] The masonry assemblies were fabricated from the batches of bricks and mortar employed to construct the buildings; all tests were performed on specimens of an age exceeding 28 days. Table 1 summarizes the estimated mechanical properties of masonry (i.e., average values and dispersions) for each building specimen. The data shows some inter-building variability of the mechanical characteristics, especially those related to the bond strength between mortar and brick, even though the same bricklayers constructed the specimens alongside and under controlled conditions. For instance, buildings EUC-BUILD-8.2 and EUC-BUILD-8.3 exhibited around 30%–40% higher bed-joint cohesion but 40% weaker tensile bond strength than EUC-BUILD-8.1. Nonetheless, such differences are near enough the variability found within each specimen (i.e., intra-building variability). For further information on the adopted test procedures and a detailed reporting of the material test results, the reader is referred to Kallioras et al.[26]

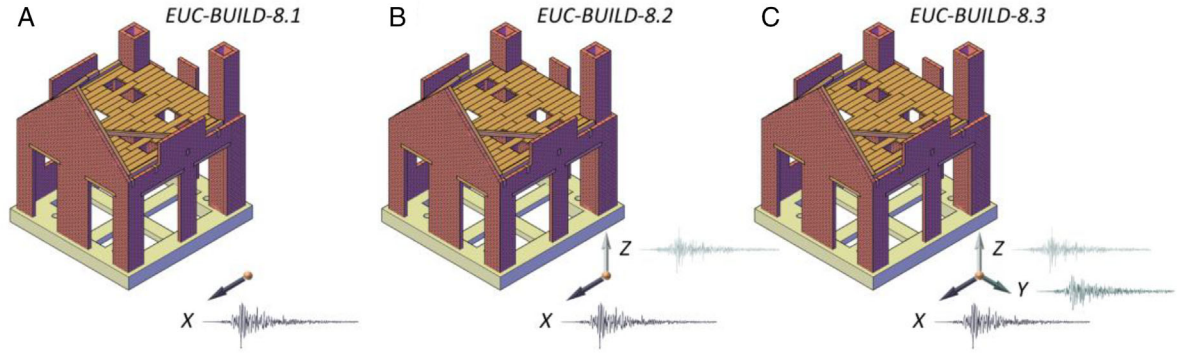

FIGURE 3 Incremental dynamic shake-table testing: application of (A) uni-, (B) bi-, and (C) tri-directional seismic excitations. Arrows indicate the direction of shaking

3 | SHAKE-TABLE TESTS

The building specimens were subjected to cumulative incremental dynamic tests, applying a series of shake-table motions of increasing intensity to assess damage evolution, failure modes, and ultimate structural capacity under multidirectional shaking. The same seismic input was adopted for all experiments, every time introducing one additional motion component (Figure 3). In particular, EUC-BUILD-8.1 was subjected to unidirectional excitations by applying the principal horizontal acceleration component alone. EUC-BUILD-8.2 was subjected to bidirectional excitations by combining the principal horizontal and vertical acceleration components. Finally, EUC-BUILD-8.3 was tested under all three components simultaneously. The same instrumentation plan was adopted for all specimens; it consisted of 65 accelerometers, 22 linear and 17 wire potentiometers, and a three-dimensional optical motion-capture system monitoring the dynamic response in horizontal and vertical directions. This practice allowed the direct comparison of the data obtained from the three experiments. All data, including conventional and optical measurements, are available upon request on www.eucentre.it/nam-project.

3.1 | Seismic input motions

Two real earthquake scenarios were considered in the experiments: ground motions due to anthropogenic and tectonic activity. Figure 4 illustrates the theoretical three-component acceleration time-series of the two input ground motions and their elastic pseudo-acceleration response spectra for a 5% viscous damping ratio. The plots also show the ground velocities (within shaded boxes) and the predominant velocity pulse (in red) extracted using wavelet analysis.[29]

The first motion, labeled SC1, was a three-component, pulse-like acceleration recording from the 2018 Zeerijp earthquake (M_W 3.4) in the Groningen gas field of the Netherlands.[30,31] Earthquakes caused by gas production activities are typically characterized by shallow depth and low magnitude. Consequently, they usually generate vertical and horizontal ground motions of comparable intensities but with a low amplitude and short duration. In record SC1, the principal horizontal and vertical motions had peak amplitudes of 0.11 and 0.071 g, which were not synchronized. The short source-to-site distance (R_{ep} = 2.5 km and D = 3 km) resulted in a considerable time lag between the arrival of vertical and horizontal motions at the site. In the near field, vertical shaking is predominantly associated with vertically propagating P waves (i.e., direct P and S-to-P converted waves), while horizontal ground shaking is mainly caused by S waves (in the far-field, Rayleigh waves may also contribute).[32,33] Since the P-wave velocity is always higher than the S-wave velocity—that is, in the Groningen gas field, V_P is over two times greater than V_S[34]—the peak vertical acceleration preceded the horizontal one by nearly 2 s. This was a long time interval considering the short significant duration of the two motion components (less than 1.5 s).

The second ground motion scenario, termed SC2, was a three-component accelerogram recorded near the causative fault of the October 26 event (M_W 5.9) of the 2016 Central Italy earthquake sequence, nearby Visso.[35,36] This ground motion was preferred among a suite of 10 earthquake records from near-fault sites proposed by Özcebe et al. for the shake-table tests.[37] The earthquakes were carefully selected from the NESS database (NEar-Source Strong-motion database[38]), aiming at vertical and horizontal ground motions of high amplitudes and synchronized peaks. The main horizontal and vertical

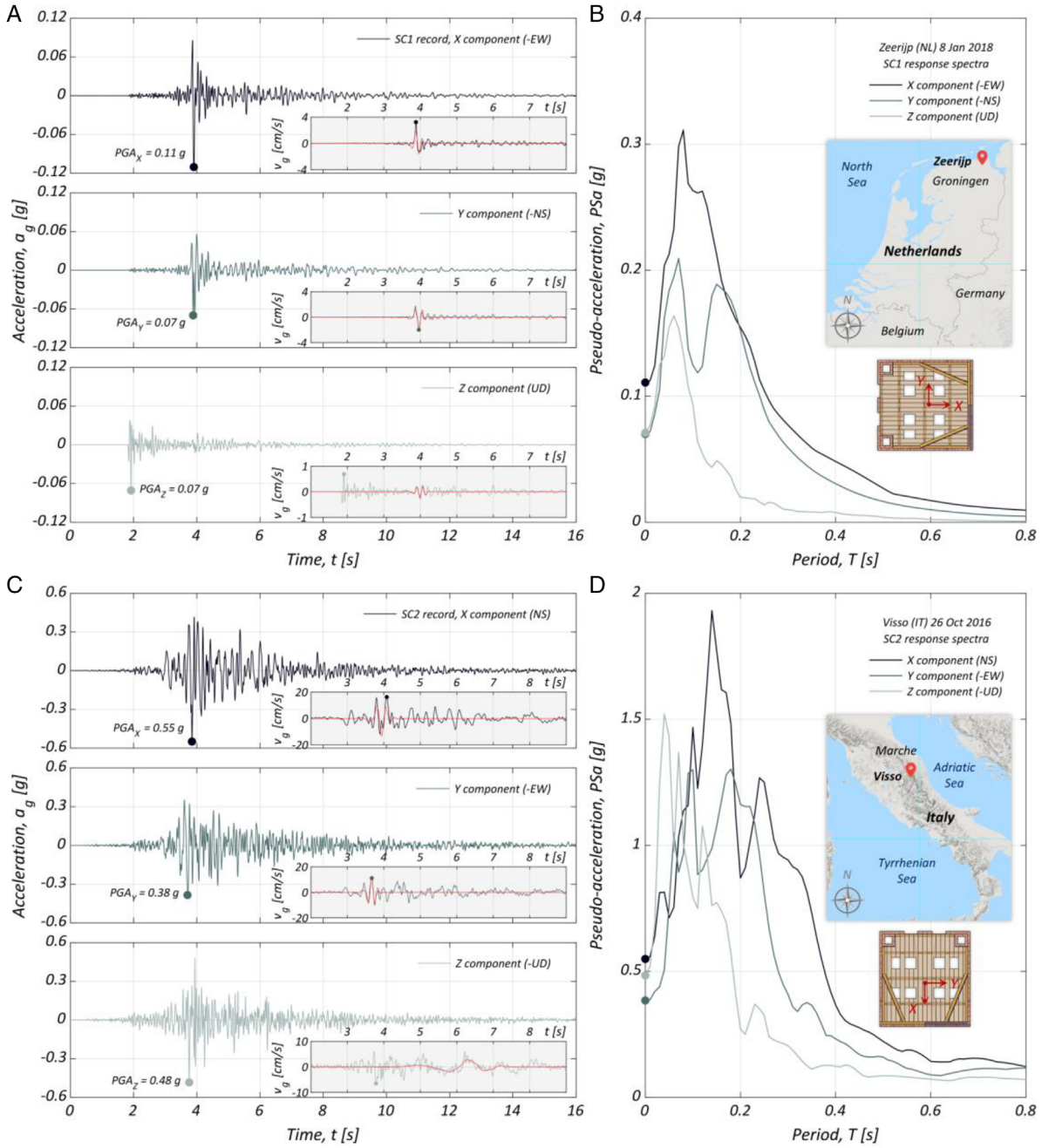

FIGURE 4 Theoretical input motions SC1 and SC2: (A, C) acceleration and velocity time-series; (B, D) elastic pseudo-acceleration response spectra for 5% viscous damping ratio and notional building orientation at the field

acceleration components of record SC2 had peak amplitudes equal to 0.55 and 0.48 g, respectively, while the time interval between the two peaks was just 0.09 s, with the vertical arriving first.

All dynamic tests were performed by applying the principal horizontal acceleration component in the X building direction. The peak acceleration was directed towards South (-X) to induce an outward out-of-plane overturning mechanism of the North gable wall. This element was generally most vulnerable when subjected to Southward pulses since the truss restrained its motion toward the inside. Therefore, ground motion SC1 was rotated 90° counterclockwise on the horizontal plane to align the E–W and N–S components with the N–S (-X) and W–E (-Y) building directions, respectively. Similarly, motion SC2 was rotated through 180° on the horizontal plane so that the E–W and N–S components coincided with the W–E (-Y) and S–N (+X) building directions.

TABLE 2 Characteristics of the selected ground motions and measures of the relative V/H motion intensity

Event	Date and time	Station	M_W (–)	R_{ep} (km)	D (km)	PGA_V/PGA_H[a] (–)	PGV_V/PGV_H[a] (–)	$PSa_{V,avg}/PSa_{H,avg}$[a] (–)	$I_{A,V}/I_{A,H}$[a] (–)	$\Delta t_{IA,5\%}$[b] (s)
Zeerijp, Netherlands	08/01/2018, 14:00:52 (UTC)	Garsthuizen (BGAR) Lat: 53.368, Long: 6.714	3.4	2.5	3.0	0.81	0.27	0.74	0.35	1.97
Visso, Central Italy	26/10/2016, 19:18:06 (UTC)	Montecavallo (MCV) Lat: 42.909, Long: 13.129	5.9	14.0	7.5	1.05	0.48	1.07	0.66	0.22

[a]Quantity H was computed as the geometric mean of the quantities for the two orthogonal horizontal components, X and Y; the geometric mean of quantities Q_X and Q_Y is equal to the square root of their product, that is, $Q_H = \sqrt{Q_X Q_Y}$.
[b]Time difference provided in absolute value; $t_{IA,5\%}$ of the vertical motion precedes that of the principal horizontal motion in both selected ground motion sets.

Moreover, the polarity of the vertical acceleration component of ground motion SC2 was inverted with respect to the one recorded originally so that the peak pointed downwards. This adjustment was made deliberately to reduce the gravity loads, and consequently, the in-plane shear resistance of piers and the restoring moment of free-standing masonry elements at the instant of peak horizontal shaking. Nonetheless, it was verified that changing the vertical motion polarity was still compatible with the seismotectonic setting and focal mechanisms characterizing earthquakes in Central Italy, which are typically generated by normal faulting systems (extensional tectonic regime[39]).

Table 2 lists information regarding the location of the accelerometric stations that recorded the two selected ground motions (i.e., geographic coordinates; epicentral distance, R_{ep}) and the main seismological parameters characterizing the corresponding quakes (i.e., moment magnitude, M_W; focal depth, D). The table also provides various engineering measures of the relative intensity and synchronization of the vertical and horizontal ground motion components. Among these measures, the ratios of peak vertical to peak horizontal ground accelerations, PGA_V/PGA_H, and peak vertical to peak horizontal ground velocities, PGV_V/PGV_H, are two commonly referred indicators of the relative energy content at the short- and intermediate-period ranges, respectively.

A more accurate estimate of the relative V/H seismic demand to structures is provided by the V/H response spectra ratio. Herein, the V/H spectral ratio was taken as the average vertical to average horizontal pseudo-accelerations, $PSa_{V,avg}/PSa_{H,avg}$. Quantities $PSa_{V,avg}$ and $PSa_{H,avg}$ were calculated over the period ranges 0.05–0.15 s and 0.10–0.35 s, respectively, at spacing 0.01 s and for a 5% damping ratio. The two different period windows represent natural vibration periods of typical low-rise URM buildings (like specimens EUC-BUILD-8) for response in the vertical and horizontal directions. Additionally, the relative V/H integral intensity was accounted for by the ratio of Arias intensities of the two components, $I_{A,V}/I_{A,H}$.[40] The time difference between the 5% cumulative $I_{A,V}$ and $I_{A,H}$, termed $\Delta t_{IA,5\%}$, was used to evaluate the energy-based synchronization between vertical and (principal) horizontal motions.

3.2 | Test sequence

The seismic input signals were scaled in amplitude progressively to achieve the desired shaking intensities up to near-collapse conditions of the buildings. The nominal test protocol consisted of 10 main earthquake simulations: first, record SC1 (i.e., Zeerijp, Groningen 2018) was scaled in acceleration amplitude at 50%, 100%, and 150%; then, motion SC2 (i.e., Visso, C. Italy 2016) was scaled at 25%, 50%, 75%, 100%, 150%, and 200%, with shaking at 75% been performed twice. Test SC2-75% was a test-milestone in the development of the experiments as it brought the North gable wall close to collapse; retrofitting was required before testing at higher intensities. As each earthquake record was linearly scaled, its V/H intensity ratio and its significant duration remained unchanged.

Table 3 illustrates the applied test sequence, specifying the recorded *PGA* and *PGV*, and the actual *PSa* at the fundamental period of the damaged buildings, $T_{1,i}$. Typical single-period spectral intensity measures (IMs) like $PSa(T_{1,i})$, or *PSa* at the undamaged building period $T_{1,und}$, do not allow for an unbiased comparison of the actual seismic demands on the three specimens. In fact, $PSa(T_{1,und})$ correlates poorly with the inelastic response of the buildings, while $PSa(T_{1,i})$ might vary significantly from specimen to specimen for the same nominal shaking intensity due to differences in their damage

TABLE 3 Summary of main earthquake simulations and corresponding intensity measures of the principal horizontal ground motion component (i.e., in the X building direction)

Test ID	Rec. *PGA* (g)			Rec. *PGV* (cm/s)			$PSa(T_{1,i})$ (g)			PSa_{avg} (g)			I_A (cm/s)			*CAV* (cm/s)			$I_{H,m}$ (mm)		
	B8.1	B8.2	B8.3	B8.1	B8.2	B8.3	B8.1	B8.2	B8.3	B8.1	B8.2	B8.3	B8.1	B8.2	B8.3	B8.1	B8.2	B8.3	B8.1	B8.2	B8.3
SC1-50%	0.051	0.066	0.082	1.3	1.5	1.6	0.11	0.13	0.14	0.052	0.066	0.085	0.26	0.53	0.95	20	42	63	5.9	5.8	8.4
SC1-100%	0.12	0.13	0.14	3.0	3.6	3.7	0.24	0.29	0.32	0.12	0.18	0.17	1.4	2.1	2.2	42	62	61	14	17	17
SC1-150%	0.18	0.17	0.17	4.8	4.9	4.6	0.36	0.35	0.35	0.19	0.23	0.21	4.0	4.3	4.6	72	99	111	22	20	22
SC2-25%	0.13	0.14	TNP	3.9	4.8	TNP	0.38	0.49	TNP	0.24	0.30	TNP	6.8	8.3	TNP	130	160	TNP	32	36	TNP
SC2-50%	0.30	0.27	0.23	9.1	10	7.7	0.83	0.85	0.95	0.53	0.57	0.47	36	34	24	310	350	230	71	81	63
SC2-75%	0.37	0.43	0.39	11	15	12	1.0	0.99	1.5	0.63	0.91	0.78	49	79	61	350	490	380	85	120	100
SC2-75%-bis[a]	0.38	0.43	0.36	12	15	11	1.2	0.91	0.99	0.70	0.92	0.78	61	82	70	400	490	450	96	130	95
SC2-100%	0.58	0.58	0.48	17	21	16	0.98	1.2	0.95	0.98	1.2	1.1	120	140	130	560	630	620	130	170	130
SC2-150%	0.81	0.86	0.71	23	32	23	1.4	1.8	1.5	1.4	1.8	1.6	260	310	290	870	940	940	190	250	200
SC2-200%	1.3	1.1	0.90	31	37	33	2.0	1.1	2.1	1.9	2.3	2.1	520	490	450	1200	1200	1200	260	300	250

Below each ground motion IM, the leftmost, central, and rightmost columns provide data for tests EUC-BUILD-8.1, EUC-BUILD-8.2, and EUC-BUILD-8.3, respectively—abbreviated to B8.1, B8.2, and B8.3 in the column header. Values are reported with two significant digits.

TNP: test not performed (i.e., test SC2-25% for EUC-BUILD-8.3).

[a]Test SC2-75%-bis was a repetition of the previous test (i.e., test SC2-75%).

evolution. Therefore, the table also provides the geometric mean of the pseudo-acceleration spectral ordinates, PSa_{avg}, calculated in the period window from $0.2T_{1,und}$ to $3T_{1,und}$ at spacing 0.01 s.[41] For convenience in calculating the PSa_{avg}, $T_{1,und}$ was set equal to 0.12 s for all three specimens.

Several other ground motion IMs were computed to describe the damage potential of the applied shake-table motions. In particular, Table 3 lists the conventionally defined cumulative absolute velocity, *CAV*, and Arias intensity, $I_{A.}$[40,42] Due to their integral definition, both IMs can simultaneously reflect the cumulative effects of ground motion amplitude, duration, and frequency content (i.e., the integrand value between zero-crossings is frequency-dependent). Table 3 also provides a modified definition of the Housner intensity,[43] represented by $I_{H,m}$: it was evaluated as the integral of the 5%-damped pseudo-velocity spectrum between 0.1 and 0.5 s since the fundamental period of the examined structures falls within this range.[44] This spectral IM has proved to correlate well with inelastic displacement demands on short-period URM structures.[45,46]

The 5%–75% and 5%–95% significant durations, $D_{s,5\text{-}75}$ and $D_{s,5\text{-}95}$, were preferred to describe the ground motion duration. They were calculated as the time intervals between the development of 5% and 75% of I_A, and between 5% and 95% of I_A, respectively.[47,48] The principal horizontal component of motion SC1 had nominal $D_{s,5\text{-}75} = 0.43$ s and $D_{s,5\text{-}95} = 3.32$ s, while signal SC2 had nominal $D_{s,5\text{-}75} = 1.87$ s and $D_{s,5\text{-}95} = 4.26$ s. The significant duration of the vertical ground motion components was noticeable longer: motion SC1 had $D_{s,5\text{-}75}$ and $D_{s,5\text{-}95}$ of 1.54 s and 4.48 s, while SC2 had $D_{s,5\text{-}75}$ and $D_{s,5\text{-}95}$ of 2.10 s and 5.34 s. Note that short durations characterized both selected earthquake records due to their short epicentral distance (2.5 km for SC1; 14 km for SC2).

Comparisons between the target response spectra and those obtained from accelerations recorded at the foundation of the specimens showed that the controller reproduced the ground motions generally well. A slight overshoot was only observed for building EUC-BUILD-8.2 when subjected to motion SC2 scaled at amplitudes over 25%. In particular, the actual horizontal shaking intensity was on average 10% higher than the expected one in terms of PSa_{avg} between 0.024 and 0.36 s periods. This distance between actual and target spectral ordinates can partially explain why EUC-BUILD-8.2 exhibited structural damage before the other two building specimens. The performance of the shake-table tests was deemed satisfactory also in terms of vertical response spectra. An undershoot of 30%–40% was noticed for the vertical accelerations only during tests SC2-50% and SC2-75% on EUC-BUILD-8.3.

4 | TEST RESULTS

4.1 | Observed damage mechanisms—Retrofit of North wall

Each building specimen was first subjected to the series of induced earthquakes SC1, followed by simulations of the stronger tectonic ground motion scenario SC2. Consequently, the seismic behavior of the buildings under earthquakes SC2 was inevitably affected by minor pre-existing damage induced by motions SC1. Detailed illustrations of the observed crack patterns can be found in the technical report of Kallioras et al.[26]

Buildings EUC-BUILD-8.1 and EUC-BUILD-8.3 suffered only slight structural damage under earthquakes SC1, that is, up to test SC1-150% (nominal $PSa_{X,avg} = 0.21$ g and $PSa_{Z,avg} = 0.14$ g). Hairline cracks appeared mostly at the interfaces between masonry and timber elements (lintels and floor joists) and the spandrels of the West façade. The first noteworthy damage to the two specimens was observed during tests SC2-25% ($PSa_{X,avg} = 0.26$ g; $PSa_{Z,avg} = 0.24$ g) and SC2-50% ($PSa_{X,avg} = 0.53$ g; $PSa_{Z,avg} = 0.47$ g), respectively. Flexural-tensile cracks developed at the bottom of the West piers, associated with their in-plane flexural-rocking behavior. In the same tests, the slender chimney of both buildings fractured (through flexure) at the level where it penetrated the floor and initiated rocking over a height of about 2.0 m. By the end of test SC2-50%, an out-of-plane overturning mechanism involving the North gable wall had been activated in both buildings. None of the parapet walls of specimen EUC-BUILD-8.3 were damaged until this intensity level; in contrast, the South parapet of EUC-BUILD-8.1 cracked during test SC2-25%.

The first significant damage to EUC-BUILD-8.2 was noticed after test SC1-100% ($PSa_{X,avg} = 0.14$ g; $PSa_{Z,avg} = 0.09$ g) and was diffused all over the structure. Stair-stepped cracks formed on the West spandrel beams, originating from the floor beams and propagating towards the openings. Hairline cracks were found just above the North wall openings, extending along the entire façade length, compatible with incipient activation of an out-of-plane overturning mechanism of the gable. Horizontal flexural cracks were also clearly visible a few centimeters below the gable tip and at the floor joints of the South parapet wall. A hairline horizontal crack appeared along the base of the East façade, associated with the development of a shear-sliding mechanism; this failure mode was also seen in EUC-BUILD-8.1 and EUC-BUILD-8.3 but

in later tests (i.e., at SC2-25% and SC1-150%, respectively). Shaking at SC2-50% caused vertical cracks on the West spandrel beams and a horizontal flexural crack at the base of the slender chimney, which activated a rocking response mechanism involving the entire South-West building corner.

In EUC-BUILD-8.2, shaking at SC2-50% caused a new horizontal crack at the gable mid-height and collapse of the gable upper part, which tipped on the timber plate installed outside the wall. Therefore, the North façade was retrofitted before proceeding with shaking tests of higher intensity to prevent premature termination of the experiment due to a local collapse mechanism. The strengthening interventions included: (i) activating the four (up to that moment idle) wall-to-diaphragm steel connectors; and (ii) fixing the timber end-plate tightly outside the gable. In contrast, for specimens EUC-BUILD-8.1 and EUC-BUILD-8.3, the retrofit system was activated only after tests SC2-75% and SC2-75%-bis, respectively (nominal $PSa_{X,avg} = 0.79$ g; $PSa_{Z,avg} = 0.71$ g). In EUC-BUILD-8.3, testing at SC2-75% induced flexural cracking of the South parapet wall at 20 cm above the floor diaphragm.

Earthquake SC2-100% ($PSa_{X,avg} = 1.1$ g; $PSa_{Z,avg} = 0.94$ g) caused stair-stepped cracking of the East corner piers in all three specimens. The cracks were initiated by the participation of the piers in the out-of-plane response of the North and South façades. During test SC2-150% ($PSa_{X,avg} = 1.6$ g; $PSa_{Z,avg} = 1.4$ g), extensive damage to the spandrels was observed in both longitudinal façades. This test induced the South parapet wall collapse in EUC-BUILD-8.1 and fracture at the floor level of the slender chimney in EUC-BUILD-8.2. All three specimens were brought into near-collapse conditions during test SC2-200% ($PSa_{X,avg} = 2.1$ g; $PSa_{Z,avg} = 1.9$ g) when parts of the West and North façades had lost their load-bearing capacities. Shaking at SC2-200% also caused the collapse of the South parapet wall in EUC-BUILD-8.2. The buildings would have hardly survived further shaking; therefore, tests were stopped to prevent collateral damage to the instrumentation and the shake table.

4.2 | Global dynamic response

4.2.1 | Vibration period evolution

The specimens were subjected to low-amplitude random excitations covering a wide frequency band (i.e., 0.1–40 Hz) with consistent energy content for dynamic identification between the main earthquake tests. The fundamental vibration periods in the X direction of the undamaged buildings were $T_{1,und} = 0.13$ s, 0.10 s, and 0.12 s (in frequencies, $f_{1,und} = 7.7$ Hz, 10 Hz, and 8.3 Hz), while by the end of all tests they had shifted to $T_{1,dam} = 0.26$ s, 0.39 s, and 0.25 s ($f_{1,dam} = 3.8$ Hz, 2.6 Hz, and 4.0 Hz), respectively, for EUC-BUILD-8.1, EUC-BUILD-8.2, and EUC-BUILD-8.3. In the Z direction, the vibration period was 0.05 s, and it did not vary during the test sequence. Modal frequencies were estimated by analyzing the frequency response functions established using recordings from accelerometers mounted at the foundation and the floor level of the perimeter masonry walls (blue dots in the sketches of Figure 5 indicate the locations of sensors on the North and West façades). Accelerometers were also mounted at the center and the East and West edges of the floor to monitor vertical vibrations of the diaphragm, which had a period equal to 0.12 s.

The bottom plot in Figure 5 shows the evolution of the first-mode period for response in the X direction, estimated at the end of the annotated earthquake simulations. One can observe that the period of EUC-BUILD-8.2 increased faster than the other two specimens. The first substantial change was observed during test SC2-50% when the period reached 0.24 s: the South-West portion of the building, including the slender chimney, separated from the rest of the structure due to the formation of vertical cracks in the spandrels. Further significant elongation to 0.33 s was reported after test SC2-75% when cracks developed at the top and bottom ends of the North piers due to interaction between the in-plane and out-of-plane responses of intersecting walls. The wall-to-diaphragm connections at the North façade had already been activated, and they are believed to have promoted a global response of the structure. Different from EUC-BUILD-8.2, the periods of EUC-BUILD-8.1 and EUC-BUILD-8.3 exhibited similar trends across the same (nominally) test sequence. Discrepancies in the damage evolution of EUC-BUILD-8.2 can be partially explained by the unintended higher shaking intensities applied to it, as indicated by the values provided in Table 3.

Figure 5 illustrates the correlation between the period evolution and the cumulative energy imparted to the three specimens in horizontal and vertical (where applicable) directions across the test sequence. Energy is expressed in I_A, mostly representing the high-frequency nature of a ground motion.[49] Despite the large aleatory variability associated with I_A – that is, the existing ground motion prediction equations exhibit high uncertainty in estimating I_A – once known, this IM tends to predict the seismic demands and damage to short-period structures accurately.[50] Apparently, over the entire test series, the input energy in the X direction of EUC-BUILD-8.2 was higher than EUC-BUILD-8.1 and EUC-BUILD-8.3 by

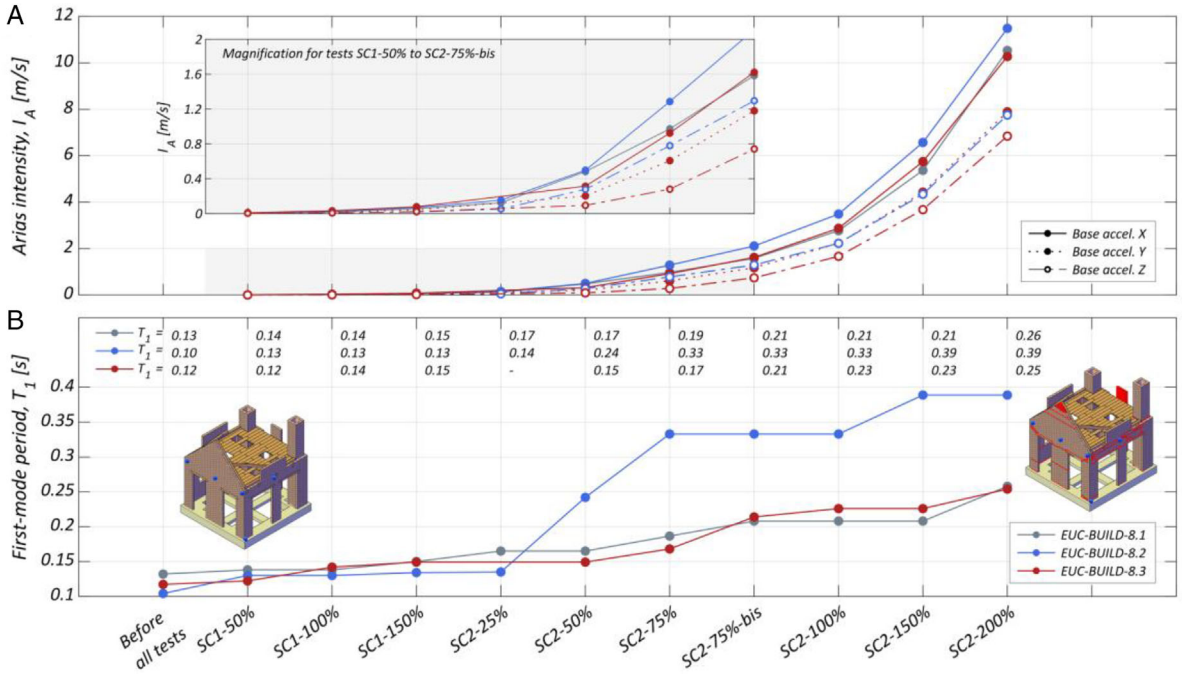

FIGURE 5 Cumulative incremental dynamic test sequence: (A) cumulative seismic input energy; (B) first-mode period evolution for response in the X building direction

9% and 12%, respectively (see solid lines in Figure 5A). The most significant differences in I_A were noticed during tests SC2-50% to SC2-75%-bis when the period of EUC-BUILD-8.2 elongated rapidly from 0.14 to 0.33 s. In those tests, the I_A of the X ground motion component to EUC-BUILD-8.2 was on average 30% greater than the other two buildings.

Discrepancies in the input energy were also observed for motion in the vertical direction (see dashed lines in Figure 5A). Specifically, the vertical ground motion series applied to EUC-BUILD-8.2 was generally 13% stronger in I_A than the vertical seismic input to EUC-BUILD-8.3. Although one could argue that the higher vertical accelerations should be the reason why EUC-BUILD-8.2 suffered more damage than EUC-BUILD-8.3, this seems not to be the case. The latter exhibited seismic performance similar to specimen EUC-BUILD-8.1, which was not subject to vertical accelerations at all. Moreover, contrary to what one might have expected, applying the second horizontal motion component to EUC-BUILD-8.3 (dotted line in Figure 5A) did not cause more significant structural damage in comparison to the other two specimens. Therefore, disparities in overall damage suffered by the three buildings were predominantly attributed to the variability in the masonry mechanical properties and local construction details or flaws.

4.2.2 | Motion amplification

Figure 6 shows the acceleration response spectra obtained from the motions recorded at the base and atop the masonry walls during earthquakes SC1-150% and SC2-200%. These two tests were selected here to demonstrate differences in the motion filtering effect of the buildings at conditions of slight structural damage and imminent collapse. As expected, the floor spectra at the East and West walls differed substantially from each other and the ground response spectra in both magnitude and shape. When the behavior was still elastic, all three specimens amplified motions around their fundamental global period in the X direction (i.e., range $T_{1,\text{und}}$ to $T_{1,i}$ shaded in gray in Figure 6A). Specifically, the East wall, including stockier piers, amplified accelerations only slightly around periods 0.05–0.10 s; in contrast, the West wall, which included larger openings, amplified accelerations around periods 0.15–0.20 s by a factor greater than three. Amplified were also the accelerations at zero periods on the floor response spectra: horizontal acceleration amplification factors (AMP_H) of 1.1–1.4 and 1.5–2.3 were observed at the East and West walls. The *AMP*s were computed here as the ratios of the peak accelerations at the floor level of the walls to the peak foundation acceleration.

In the progress of testing, peak and spectral floor accelerations were generally de-amplified with respect to the foundation accelerations, as the buildings cumulated damage and their dynamic global response transitioned from elastic to

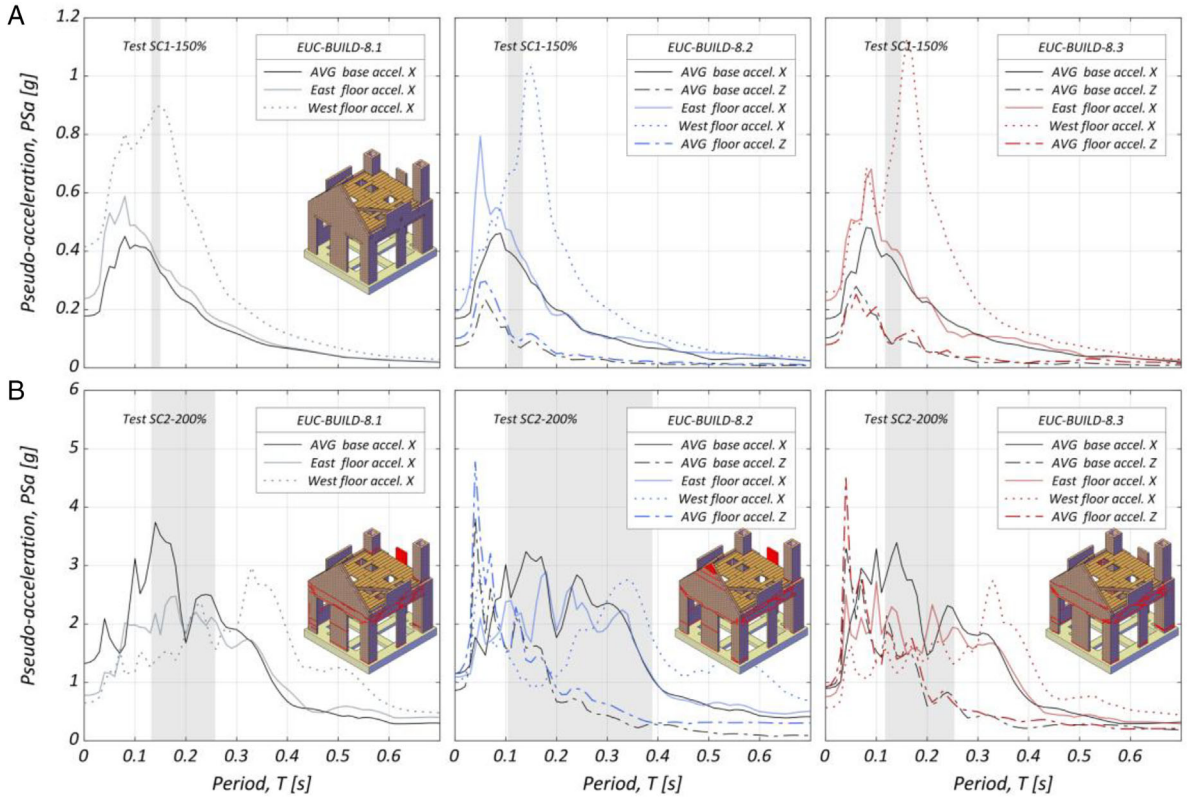

FIGURE 6 Horizontal and vertical motion amplification by the building specimens at (A) slight damage conditions (SC1-150%) and (B) near-collapse conditions (SC2-200%). Shades in gray indicate the range of fundamental period elongation

nonlinear. This is readily appreciated when one looks at the acceleration spectra from test SC2-200% in Figure 6B. The AMP_H factors for the damaged East and West walls were reduced to 0.58–0.95 and 0.49–0.87, respectively. At the West façade, acceleration amplification was only observed in the high-period range (i.e., above 0.3 s), attributed to local vibration modes of the transverse building façades and the slender chimney. In the Z direction, amplifications were observed in the short-period range since the vertical ground motion is mainly composed of high-frequency pulses, which coincide with the fundamental vertical period of the buildings (i.e., equal to 0.05 s). Under earthquakes SC2, the estimated AMP_V was on average equal to 1.2 for both EUC-BUILD-8.2 and EUC-BUILD-8.3.

4.2.3 | In-plane response of longitudinal walls

The seismic response of walls in the longitudinal building direction was examined locally considering two separate subsystems: East or *Windows* wall and West or *Doors* wall. These two parallel building façades exhibited different behaviors due to different pier geometry, combined with the flexibility of the floor-diaphragm, which provided little coupling between them.

The inter-story drift ratio induced on each subsystem was taken as the reference engineering demand parameter to describe their in-plane response. Inter-story drift ratios $\theta_{1,E}$ and $\theta_{1,W}$ were defined individually for the East and West walls, respectively, at the first-floor level: $\theta_{1,E} = \Delta_{1,E}/h_1$, and $\theta_{1,W} = \Delta_{1,W}/h_1$. In the equations, $\Delta_{1,E}$ and $\Delta_{1,W}$ are the average displacements measured at the East and West edges of the floor diaphragm with respect to the foundation, and $h_1 = 2.82$ m is the first-floor height above the foundation. Figure 7A,B shows the maximum absolute inter-story drift ratios induced on the two walls by each earthquake versus the shaking intensity in the X direction, expressed in $PSa_{g,avg}$ and CAV_g. The subscript *g* denotes *ground* as both quantities derive from the average foundation acceleration recordings. PSa_{avg} is used here as a spectral IM, while *CAV* represents the total energy imparted to the building by each ground motion. The drift-ratio demands include cumulative residual deformations from previous tests.

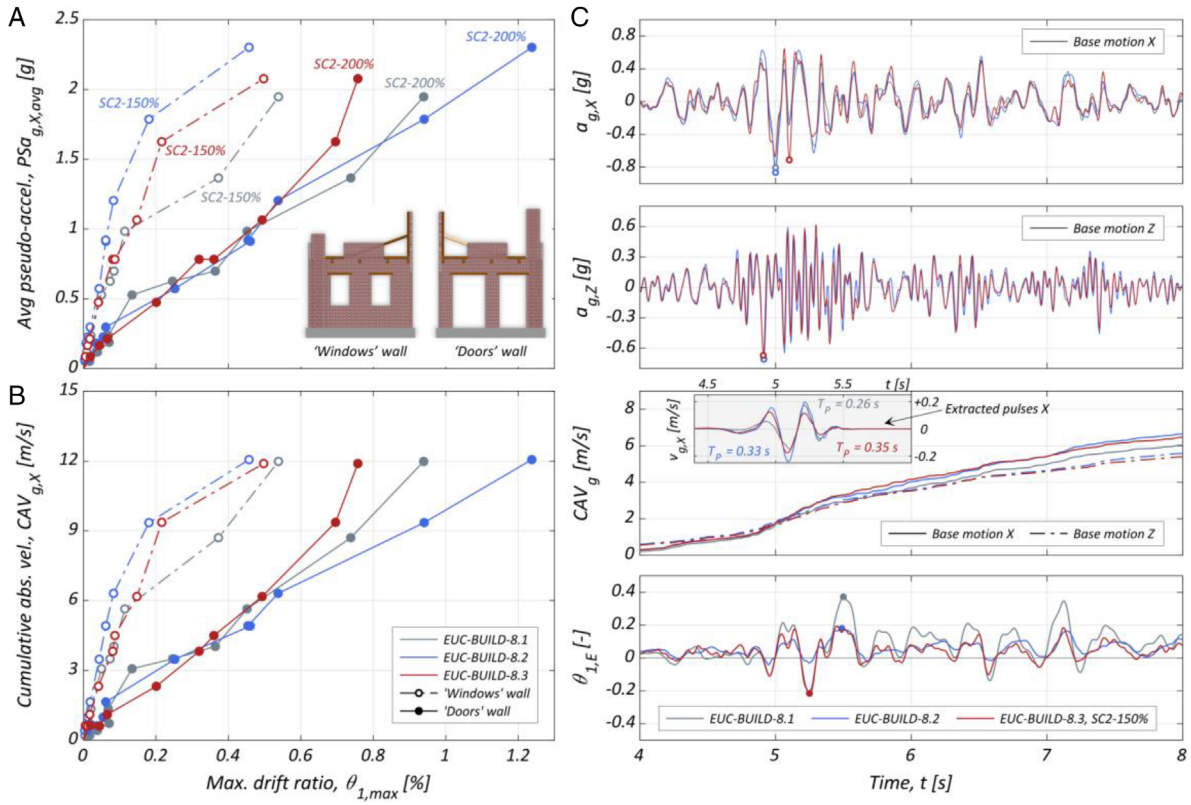

FIGURE 7 Incremental dynamic response curves of the East (*Windows*) and West (*Doors*) building walls: maximum drift-ratio demands versus (A) $PSa_{g,X,avg}$, and (B) $CAV_{g,X}$. (C) Comparison of the seismic input and response time-histories between the three East (*Windows*) walls under motion SC2-150%

The *Doors* façade, consisting of slender piers with prevailing flexural-rocking behavior, always displayed larger drift ratios than the *Windows* façade, which comprised stiffer and stronger stocky piers. Consequently, the floor diaphragm underwent significant in-plane shear deformation, which reached peak values of around 0.54% in EUC-BUILD-8.1 and EUC-BUILD-8.3 under SC2-150%, and 0.72% in EUC-BUILD-8.2 under SC2-200%. Also, all buildings exhibited a limited overall torsional response around the S–E corner (i.e., at the squat chimney location), which was more pronounced—proportionally to the magnitude of measured displacements—for EUC-BUILD-8.3 when its response was still elastic due to the second horizontal ground motion component (i.e., in the Y direction).

Differential X-displacements between the longitudinal façades of EUC-BUILD-8.2 were significantly amplified compared to the other two specimens due to large West drift-ratio responses to earthquakes SC2 (Figure 7A,B). This behavior was attributed to local failures at the West spandrel beams and the consequent cumulation of residual deformations rather than vertical accelerations, which did not affect in like manner EUC-BUILD-8.3. On the other side, the *Windows* wall of EUC-BUILD-8.1 displayed a considerably greater drift-ratio demand under SC2-150% but for reasons not evidently associated with beneficial effects of the vertical accelerations on EUC-BUILD-8.2 and EUC-BUILD-8.3. For all buildings, the peak East wall response to earthquake SC2-150% was observed a few time-steps after a significant part of the vertical motion had elapsed. Also, no major differences were noticed in the waveforms of the horizontal input ground motions to the three specimens that could justify this discrepancy other than the considerably shorter period of the predominant velocity pulse in EUC-BUILD-8.1 (Figure 7C).

Figure 8A illustrates the in-plane hysteretic response of the (West) *Doors* wall for all earthquake simulation tests. The responses are provided in terms of acceleration recorded at the floor level ($a_{1,W}$) versus inter-story drift ratio ($\theta_{1,W}$). The acceleration was taken as the ordinary arithmetic mean of the measurements by three accelerometers mounted on the West subsystem (shown in blue on the sketches of Figure 8). Northward displacements, and consequently, drift ratios are positive. Although $\theta_{1,W}$ and $a_{1,W}$ have a phase difference of π rad, the sign of accelerations in the plots has been reversed so that the responses fall in the first and third quadrants, as per a traditional force (in this case $a_{1,W}$) versus deformation (here $\theta_{1,W}$) relationship. The plots also illustrate the backbone curve for each system: white dots represent maximum

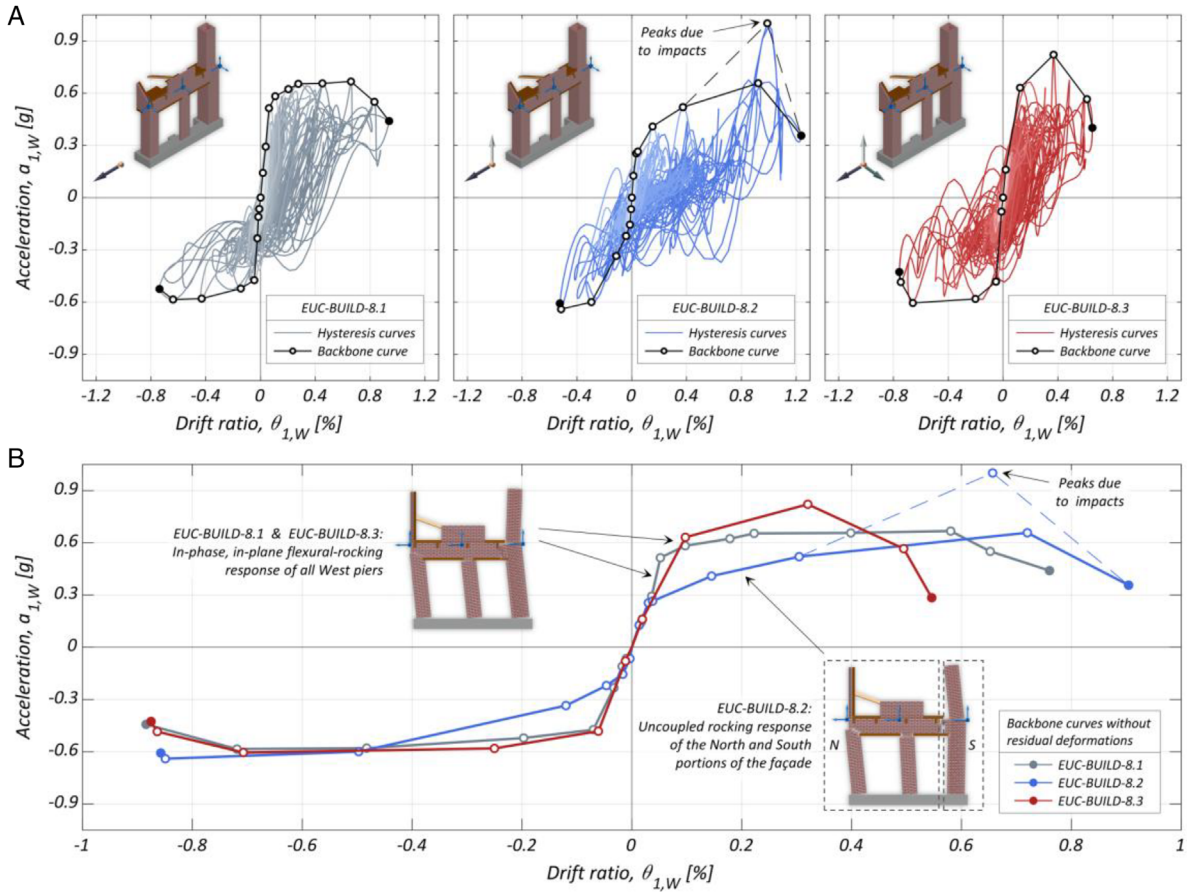

FIGURE 8 Comparison of the in-plane seismic responses of all three West (*Doors*) wall subsystems: (A) hysteretic responses; (B) backbone curves in terms of acceleration versus drift ratio

acceleration demands at every test, while the filled dot corresponds to the maximum drift-ratio demand at the final test (i.e., SC2-200%).

Notable inelastic response was initially observed in the *Doors* wall of building EUC-BUILD-8.2 during test SC2-50% ($PSa_{X,avg}$ = 0.53 g): the South-West portion of the building separated from the rest of the structure through wide vertical cracks on the spandrels. In the following tests, nonlinearities became rapidly pronounced due to the enlargement of pre-existing cracks and dislocation of masonry portions. The South part of the façade, including the slender chimney, initiated a rocking response over the entire height of the chimney independently from the North part. Consequently, acceleration readings by the instruments mounted at three different locations on the façade appeared noisy and out of phase. On the contrary, the *Doors* wall of specimens EUC-BUILD-8.1 and EUC-BUILD-8.3 exhibited nonlinear behavior for the first time during test SC2-75% ($PSa_{X,avg}$ = 0.79 g) due to the formation of horizontal flexural cracks at the bottom of the slender piers and their subsequent unison in-plane rocking response. Fluctuations in the $a_{1,W}$-$\theta_{1,W}$ curves of all specimens are almost certainly associated with higher mode or second-order effects rather than a vertical motion effect on the wall strength. Such phenomena have also been observed in previous unidirectional shake-table tests (e.g., in Refs.[27,28] and the earliest experiments by Costley and Abrams[51]).

A comparison of the backbone response curves obtained for the *Doors* wall of all three buildings is provided in Figure 8B, considering the response in both positive and negative X-directions. Drift ratios do not include residual deformations from previous tests, thus discarding traces of spurious stiffness degradation. The three structures exhibited comparable acceleration-displacement relationships for swaying to the negative direction (i.e., Southward) but differed for response in the positive direction (i.e., Northward). In particular, EUC-BUILD-8.2 displayed remarkable strength and stiffness degradation after test SC2-50% due to the local mechanism detailed previously. In test SC2-200%, the asynchronous oscillation of masses and consequent impacts caused some acceleration spikes that should not be regarded as beneficial effects of the vertical motion on the lateral strength. In contrast, EUC-BUILD-8.1 and EUC-BUILD-8.3 attained similar maximum accelerations at the various earthquake simulations.

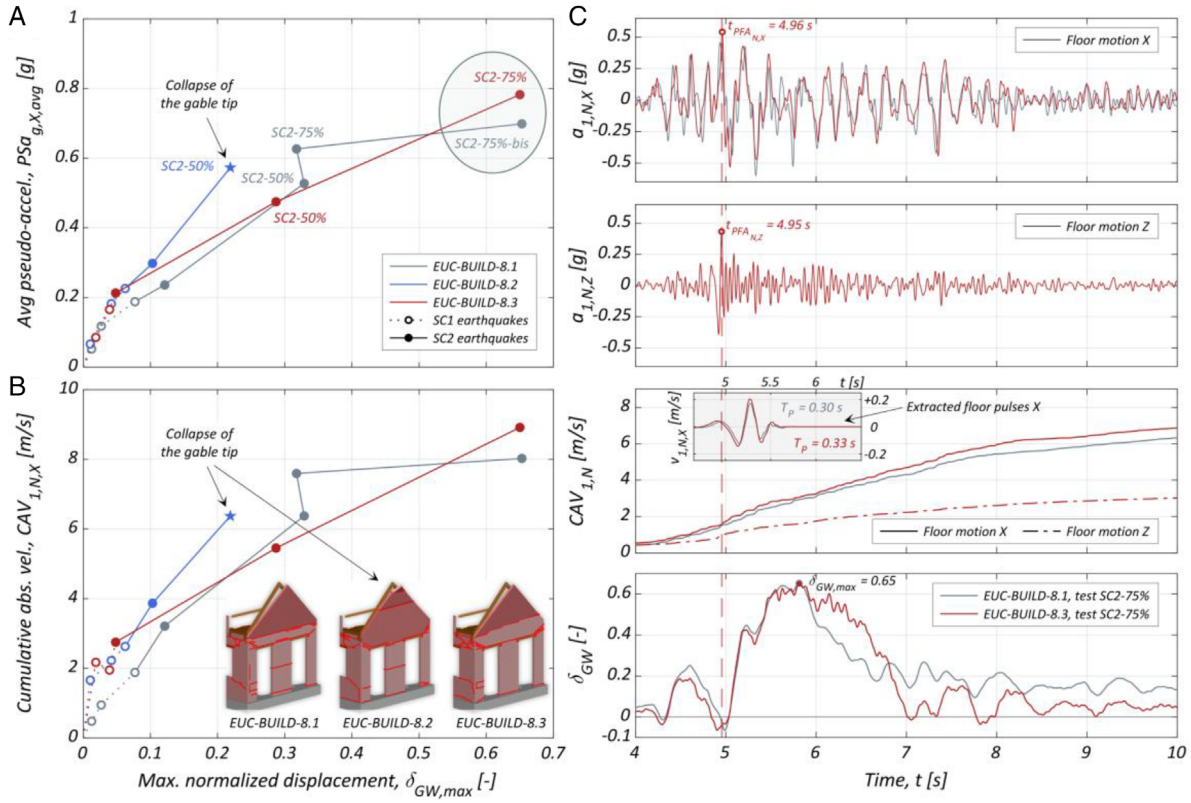

FIGURE 9 (A, B) Incremental dynamic response curves of the one-side-rocking gable: $\delta_{GW,max}$ versus $PSa_{g,X,avg}$ and $CAV_{1,X}$. (C) Comparison of the seismic input and response time-histories between gables EUC-BUILD-8.1 and EUC-BUILD-8.3

Hysteretic plots are provided here only for the West (*Doors*) subsystem, which exhibited an almost bilinear inelastic response, indicative of pier rocking. The response of the East (*Windows*) subsystem was predominantly linear elastic due to the high in-plane strength and stiffness of its stocky piers. The deformation capacity of the wall was not fully exploited, and therefore, it developed only moderate damage. The wall exhibited a combined rocking-sliding damage mechanism only during the last few tests when the corner piers participated in the out-of-plane response of the transverse building façades. This behavior did not allow detecting any potential beneficial or adverse effects of the vertical motion on the in-plane shear response of the wall. Finally, to date, data analysis from these tests has not revealed damage explicitly associated with the interaction between the in-plane and out-of-plane response of walls.

4.3 | Local dynamic response

In these shake-table experiments, special attention was dedicated to investigating the impact of vertical accelerations on the stability of free-standing structural/nonstructural masonry components. This section illustrates the effects of the combined horizontal and vertical shaking on the rocking response of the North gable, South parapet, and slender chimney of the buildings. In what follows, responses are provided in terms of normalized displacements, defined as the ratio of the differential X-displacements between the top and bottom points of the developed overturning mechanisms to the wall-element thickness. The measurements were obtained from the optical motion-detection system or by wire potentiometers when data from the first was noisy.

4.3.1 | One-side rocking response: North gable wall

Figure 9A,B compare the maximum displacement responses of the one-side-rocking gable walls up to tests SC2-75%, SC2-50%, and SC2-75%-bis for specimens EUC-BUILD-8.1, EUC-BUILD-8.2, and EUC-BUILD-8.3, respectively. After these

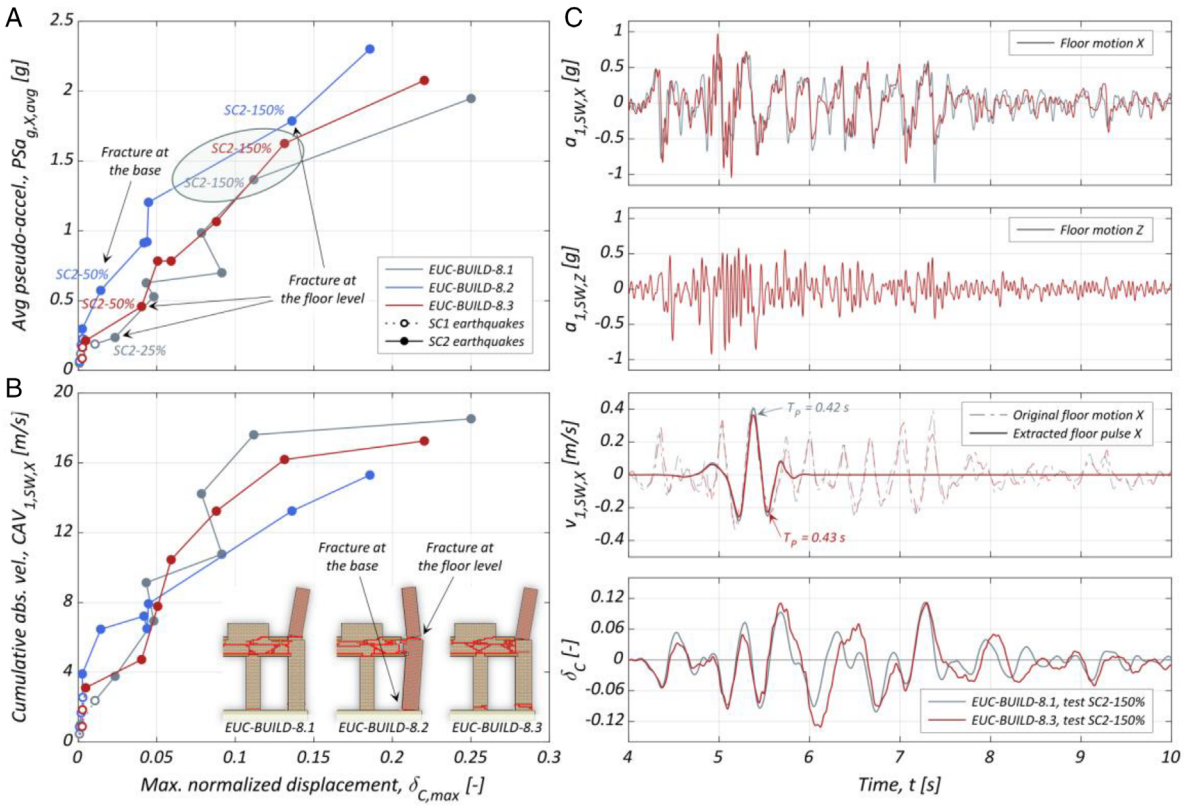

FIGURE 10 (A, B) Incremental dynamic response curves of the slender chimneys: $\delta_{C,max}$ versus $PSa_{g,X,avg}$ and $CAV_{1,X}$. (C) Comparison of the seismic input and response time-histories between chimneys EUC-BUILD-8.1 and EUC-BUILD-8.3

tests, the North building façade was retrofitted to prevent overturning of the gable. Displacements were calculated considering the bottom pivot point of the overturning mechanism at the floor-gable joint. In symbols: $\delta_{GW} = (\Delta_{GW,G} - \Delta_{1,N})/b_{GW}$, where $\Delta_{GW,G}$ is the X-displacement at the center of mass of the gable (i.e., at one-third of the distance from the floor to the ridge), $\Delta_{1,N}$ is the X-displacement at midspan of the North wall at the floor level, and $b_{GW} = 100$ mm is the thickness of the wall.

Figure 9C illustrates time-histories of the input accelerations (at the floor level) and the one-side-rocking response for the gables of EUC-BUILD-8.1 and EUC-BUILD-8.3 during tests SC2-75% and SC2-75%-bis, respectively. Interestingly, the two gable walls exhibited similar responses despite the presence of vertical accelerations in the latter case. Deviations in the post-peak response were likely due to small differences in the horizontal input motion energy to the elements (evident in the CAV_1 buildup) or the slightly longer period of the distinguishable velocity pulse at the floor level of gable EUC-BUILD-8.3.

4.3.2 | Free rocking response: slender chimney and South parapet

The two chimneys (i.e., squat and slender) exhibited dissimilar dynamic behaviors and ultimate failure modes due to their different geometry and location in the buildings. The squat chimneys of EUC-BUILD-8.1 and EUC-BUILD-8.2 fractured in shear in a brittle manner above the floor diaphragm only during the final test (i.e., SC2-200%), when accelerations at the top reached 1.6 and 1.7 g, respectively. Their response up to that point was not noteworthy and thus is not further discussed here.

Figure 10A,B shows the evolution of the peak normalized displacement demands on the slender chimneys during the test sequence. Responses are provided in the X direction only, although the EUC-BUILD-8.3 chimney underwent rocking motion in both orthogonal horizontal directions, with a consequent sliding and torsional response. Normalized displacements were derived considering only the part extending above the floor diaphragm. In symbols: $\delta_C = (\Delta_{C,t} - \Delta_{C,1})/b_C$, where $\Delta_{C,t}$ and $\Delta_{C,1}$ are the X-displacements at the top and floor level of the chimney stack, and $b_C = 540$ mm is the outer

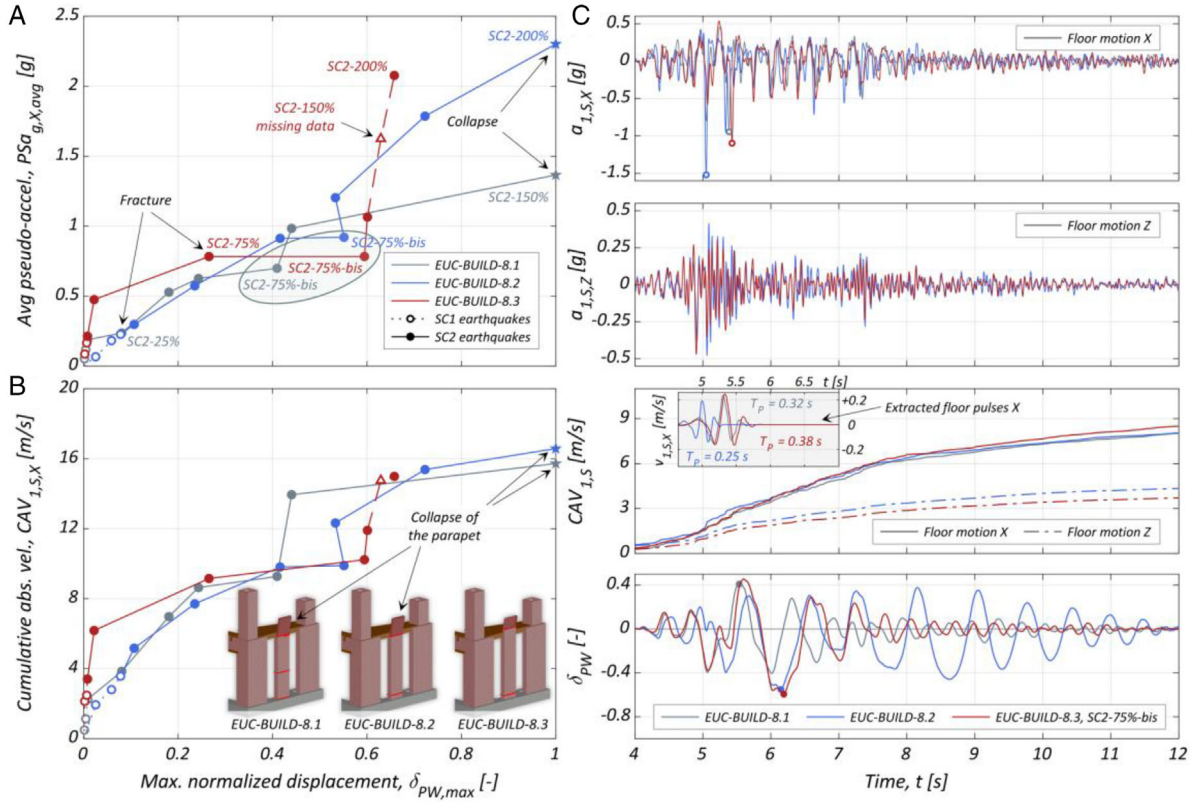

FIGURE 11 (A, B) Incremental dynamic response curves of the South parapet walls: $\delta_{PW,max}$ versus $PSa_{g,X,avg}$ and $CAV_{1,X}$. (C) Comparison of the seismic input and response time-histories between the parapets of the three buildings

width of the rectangular box section of the chimney. All chimneys enjoyed ample seismic stability as $\delta_{C,max}$ stayed well below 1.0, even at near-collapse conditions of the buildings.

The slender chimneys of buildings EUC-BUILD-8.1 and EUC-BUILD-8.3 developed flexural cracks a few centimeters above the diaphragm at early stages of the experiments (i.e., during SC2-25% and SC2-50%, respectively). In contrast, the chimney of EUC-BUILD-8.2 initially exhibited a rocking response mechanism over its full height (activated at SC2-50%), involving the entire South-West corner of the building. Cracking at the floor-chimney joint occurred during test SC2-150% when the floor-level acceleration reached 1.1 g. This delay in developing the overturning mechanism in the EUC-BUILD-8.2 chimney does not seem to be associated with the seismic input, but it was likely due to possible local irregularities in mechanical properties and construction details.

Figure 10C illustrates the responses of chimneys EUC-BUILD-8.1 and EUC-BUILD-8.3 under earthquake SC2-150%. The two elements underwent comparable rocking oscillations to almost identical horizontal input excitations at their base. The latter is also confirmed by the coincidence of the predominant velocity pulses extracted from the floor-level recordings, which had the same amplitude and period (nearly 0.4 m/s and 0.42 s, respectively). Thus, the vertical acceleration component did not considerably influence the response of the EUC-BUILD-8.3 chimney. It is worth mentioning that, in cases where the horizontal velocity pulses displayed differences in amplitude, frequency, or arrival times, the displacement response of the three chimneys deviated considerably. This verifies the claims by Makris and Konstantinidis[52] and Vassiliou et al.,[53] for the sensitivity of the dynamic response of rocking blocks to small variations of input accelerations.

Parapets EUC-BUILD-8.1 and EUC-BUILD-8.2 collapsed during shaking at SC2-150% and SC2-200%, respectively, while only parapet EUC-BUILD-8.3 survived all tests. Figure 11A,B shows the peak responses of the South parapet walls; displacements are defined as $\delta_{PW} = (\Delta_{PW,t} - \Delta_{PW,1})/b_{PW}$, where $\Delta_{PW,t}$ and $\Delta_{PW,1}$ are the X-displacements at the top and floor level of the parapet wall, and $b_{PW} = 100$ mm is the parapet breadth.

Figure 11C compares the seismic input at the floor level and the displacement response-histories of the three parapets under earthquake SC2-75%-bis. Parapets EUC-BUILD-8.2 and EUC-BUILD-8.3 attained comparable peak displacements, which were about 40% greater than EUC-BUILD-8.1. Although vertical accelerations might have caused some displacement amplification at high shaking intensities, they cannot exclusively explain the differences between the three parapet

responses. Specifically, parapet EUC-BUILD-8.2 exhibited longer rocking oscillations that lasted several seconds after the motion in the vertical direction was significantly attenuated. This behavior was also observed in other tests and was attributed to the softening of the masonry material at the floor-parapet joint under repeated oscillations since the parapet had cracked early in the test sequence. Instead, parapet EUC-BUILD-8.3 appeared more stable, demonstrating rocking motion similar to that of EUC-BUILD-8.1. Some deviations between the post-peak responses of the two were probably due to differences in the horizontal floor motion characteristics (e.g., differences in the dominant frequency of the extracted floor pulses) and the slenderness of the two elements.[52,53]

5 | DISCUSSION AND CONCLUDING REMARKS

This paper discusses one of the first experimental studies to investigate the effect of combined horizontal and vertical ground shaking on unreinforced masonry structures. The experiments comprised a series of cumulative incremental shake-table tests on three nominally identical buildings up to near-collapse conditions. The specimens simulated a full-scale unreinforced clay-brick masonry structure with a flexible diaphragm, a gable wall, chimneys, and parapets. Different seismic input combinations were considered, introducing one additional ground motion component as proceeding from experiment EUC-BUILD-8.1 (i.e., unidirectional horizontal excitation) to EUC-BUILD-8.2 (i.e., combined horizontal and vertical excitation), and eventually to EUC-BUILD-8.3 (i.e., tridirectional excitation).

The three specimens exhibited similar damage mechanisms and reached near-collapse conditions for testing at 200% of the strong ground motion SC2, with nominal $PGA_X = 1.1$ g and $PGA_Z = 0.96$ g. EUC-BUILD-8.2 suffered some more damage compared to the other two buildings. The foremost cause of this discrepancy was presumably variability in the mechanical properties and local construction details rather than vertical accelerations, which did not affect in like manner EUC-BUILD-8.3. It was also demonstrated that EUC-BUILD-8.2 was subjected to slightly higher actual shaking intensities, which might explain the somewhat increased displacement demands and damage to the walls. All buildings displayed considerable horizontal motion amplification, which was moderated when the response became inelastic. Acceleration amplification in the vertical direction was observed exclusively in the short-period range and remained nearly constant across the entire test sequence.

The tests showed that the in-plane behavior of masonry piers with prevailing flexural-rocking response was not affected by vertical accelerations. Specifically, the *Doors* walls of specimens EUC-BUILD-8.1 and EUC-BUILD-8.3 exhibited similar failure modes and hysteretic responses, despite the inclusion of the vertical ground motion component in the latter case. The observations can also be extended to EUC-BUILD-8.2, even though the wall suffered diffuse damage that significantly impaired its lateral load-bearing capacity early in the earthquake sequence. However, extreme caution must be exercised in interpreting this behavior: the specimens were lightweight structures, and the influence of vertical accelerations might depend upon the magnitude of the gravity loads, the geometry of piers, and the masonry compressive strength.

The above findings might not be transferable to walls displaying typical in-plane shear failure modes since there is no such evidence from these experiments. The squat East (i.e., *Windows*) piers suffered only moderate damage, which was not related to pure shear behavior but their interaction with the out-of-plane response of the transverse façades. A hairline horizontal crack, associated with shear-sliding, appeared along the base of the *Windows* wall. However, it was unlikely due to vertical shaking: this mechanism was developed in all building specimens (including EUC-BUILD-8.1) early in the test sequence when the vertical input motions to EUC-BUILD-8.2 and EUC-BUILD-8.3 were still weak. Lastly, no remarks can be made on the effect of vertical accelerations on the behavior of spandrels, although the latter should mostly be affected by forces/accelerations along the horizontal axis.

All buildings displayed significant differential displacements between parallel walls and an overall torsional response around the stiff South-East corner. This behavior was pronounced in EUC-BUILD-8.3 when the building was still elastic due to the simultaneous application of two orthogonal horizontal ground motion components. Nevertheless, the second horizontal component did not amplify maximum displacement demands and damage to EUC-BUILD-8.3 compared to the other two buildings. This observation substantiates the common practice of analyzing walls in two orthogonal building directions separately when flexible floor diaphragms are present. Different effects might be expected for buildings with rigid diaphragms where a box-type behavior usually prevails.

Interestingly, the impact of vertical accelerations on the stability of free-standing masonry elements was generally minimal. For the ground motions considered here, the relative amplitude and the arrival time of horizontal and vertical components had a limited and non-systematic effect on peak displacement responses. The reason for the marginal influence of the vertical motion component seems to be found in that it is much richer in high-frequency content with respect to the

horizontal motion. This results in several cycles of gravity load variations and, consequently, in the fluctuation of restoring forces during a single horizontal pulse, with not exclusively positive or adverse effects. Overall, the observations from the tests confirm that rocking dynamics is more sensitive to variability in the mechanical properties of walls and peculiarities of the horizontal ground motion (e.g., pulse-like traits) rather than vertical accelerations.

The high-frequency content of vertical earthquake motions might explain to a certain extent why these experiments did not show a substantial influence of vertical accelerations on the behavior of masonry walls, as forewarned by previous numerical studies on the topic. Although those studies are correct to argue that vertical accelerations might drastically reduce axial loads, thus negatively affecting the instantaneous relationship between shear-force resistance and demand, they seem to overlook that the two often vary in time with different rates. Generally, the lateral load resistance, which is sensitive to vertical accelerations, changes faster than the horizontal actions/accelerations. Therefore, even if there could be instants at which vertical accelerations cause a significant reduction to the shear strength, such short time intervals might not be enough to fully activate and sustain a failure mechanism. Further numerical investigations should concentrate on displacement-based checks with respect to meaningful damage limit states for masonry walls of lower cohesive-frictional strength, where the influence might be more pronounced. Different findings might also emerge from investigating the effects of vertical ground motions with significant long-period amplification, like those pointed out by Elgamal and He.[54]

It is recognized that one cannot infer a universal conclusion about the vertical ground motion effects on masonry structures just from these shake-table tests due to all limitations associated with such experiments, that is, the compactness of the specimens, the short floor span, the limited material variability, the only some triggered failure modes, and the lack of considerations for aging effects and seismic input randomness. Nonetheless, these experiments generated unique data that capture at full scale the in-plane and out-of-plane behavior of masonry walls under multidirectional shaking. Future work shall concentrate on deploying the data for developing and validating analytical and numerical models to evaluate the significance of vertical earthquake motions on structural response. Therefore, elaborated datasets have been made available online at the EUCENTRE repository (www.eucentre.it/nam-project).

ACKNOWLEDGMENTS

The shake-table experiments discussed in this paper were part of the EUCENTRE project '*Study of the vulnerability of masonry buildings in Groningen*' within the research framework program on hazard and risk of induced seismicity in the Groningen province of the Netherlands, sponsored by the Nederlandse Aardolie Maatschappij BV (NAM). The valuable advice of J. Uilenreef was essential to the project and is thankfully acknowledged. The authors would like to thank H. Crowley, C.G. Lai, A.G. Özcebe, and R. Pinho for their insight and contributions related to selecting the seismic input motions for the shake-table experiments. The contribution of L. Grottoli, F. Dacarro, V. Fort, M.P. Scovenna, and the technical staff of EUCENTRE, who performed the dynamic tests, was critical to accomplishing the experimental activities and is gratefully acknowledged. The authors are thankful to the technical staff of the Department of Civil Engineering and Architecture of the University of Pavia, who performed part of the material characterization tests. Thanks also go to G. Guerrini, M. Miglietta, S. Sharma and U. Tomassetti for the practical support. Part of the data post-processing work was financially supported by the ReLUIS-DPC project 2019–2021 '*Contributions to the improvement of standards for existing masonry structures*' (Working group 10) funded by the Italian Department of Civil Protection.

DATA AVAILABILITY STATEMENT

The data that support the findings of this study are available from the corresponding author upon reasonable request.

ORCID

Stylianos Kallioras https://orcid.org/0000-0002-4252-5652
Francesco Graziotti https://orcid.org/0000-0002-0223-0139
Andrea Penna https://orcid.org/0000-0001-6457-7827
Guido Magenes https://orcid.org/0000-0002-5452-1501

REFERENCES

1. Benedetti D, Carydis P. Influence of the vertical component on damage during shallow-nearfield earthquakes. *Eur Earthquake Eng*. 1999;3:3-12.
2. Papazoglou AJ, Elnashai AS. Analytical and field evidence of the damaging effect of vertical earthquake ground motion. *Earthquake Eng Struct Dyn*. 1996;25(10):1109-1137. https://doi.org/10.1002/(sici)1096-9845(199610)25:10⟨1109::aid-eqe604⟩3.0.co;2-0

3. Elnashai AS, Papazoglou AJ. Procedure and spectra for analysis of RC structures subjected to strong vertical earthquake loads. *J Earthquake Eng*. 1997;1(1):121-155. https://doi.org/10.1080/13632469708962364
4. Collier CJ, Elnashai AS. A procedure for combining vertical and horizontal seismic action effects. *J Earthquake Eng*. 2001;5(4):521-539. https://doi.org/10.1080/13632460109350404
5. Newmark NM, Blume JA, Kapur KK. Seismic design spectra for nuclear power plants. *J Power Div*. 1973;99(2):287-303.
6. Bozorgnia Y, Campbell KW. The vertical-to-horizontal response spectral ratio and tentative procedures for developing simplified V/H and vertical design spectra. *J Earthquake Eng*. 2004;8(2):175-207. https://doi.org/10.1080/13632460409350486
7. Bozorgnia Y, Campbell KW. Ground motion model for the vertical-to-horizontal (V/H) ratios of PGA, PGV, and response spectra. *Earthquake Spectra*. 2016;32(2):951-978. https://doi.org/10.1193/100614eqs151m
8. ASCE/SEI 7-16: Minimum Design Loads and Associated Criteria for Buildings and Other Structures. American Society of Civil Engineers (ASCE). Reston, Virginia, United States; 2017.
9. EN 1998-1, Eurocode 8: Design of Structures for Earthquake Resistance – Part 1: General Rules, Seismic Actions, and Rules for Buildings. European Committee for Standardization (CEN). Brussels, Belgium; 2018.
10. NTC-18: Norme Tecniche per le Costruzioni, DM 17/01/2018. Ministry of Infrastructures and Transport (MIT). Rome, Italy; 2018 (in Italian).
11. Chioccarelli E, Iervolino I. Near-source seismic demand and pulse-like records: A discussion for L'Aquila earthquake. *Earthquake Eng Struct Dyn*. 2010;39:1039-1062. https://doi.org/10.1002/eqe.987
12. Sorrentino L, Liberatore L, Decanini LD, Liberatore D. The performance of churches in the 2012 Emilia earthquakes. *Bull Earthquake Eng*. 2013;12(5):2299-2331. https://doi.org/10.1007/s10518-013-9519-3
13. Mollaioli F, AlShawa O, Liberatore L, Liberatore D, Sorrentino L. Seismic demand of the 2016–2017 Central Italy earthquakes. *Bull Earthquake Eng*. 2018;17(10): 5399-5427. https://doi.org/10.1007/s10518-018-0449-y
14. Liberatore D, Doglioni C, AlShawa O, Atzori S, Sorrentino L. Effects of coseismic ground vertical motion on masonry constructions damage during the 2016 Amatrice-Norcia (Central Italy) earthquakes. *Soil Dyn Earthquake Eng*. 2019;120:423-435. https://doi.org/10.1016/j.soildyn.2019.02.015
15. Rinaldin G, Fasan M, Noé S, Amadio C. The influence of earthquake vertical component on the seismic response of masonry structures. *Eng Struct*. 2019;185: 184-193. https://doi.org/10.1016/j.engstruct.2019.01.138
16. Di Michele F, Cantagallo C, Spacone E. Effects of the vertical seismic component on seismic performance of unreinforced masonry structures. *Bull Earthquake Eng*. 2019;18(4):1635-1656. https://doi.org/10.1007/s10518-019-00765-3
17. Bovo M, Savoia M. Evaluation of force fluctuations induced by vertical seismic component on reinforced concrete precast structures. *Eng Struct*. 2019;178:70-87. https://doi.org/10.1016/j.engstruct.2018.10.018
18. Tsiavos A, Sextos A, Stavridis A, Dietz M, Dihoru L, Alexander NA. Large-scale experimental investigation of a low-cost PVC 'sand-wich' (PVC-s) seismic isolation for developing countries. *Earthquake Spectra*. 2020;36(4):1886-1911. https://doi.org/10.1177/8755293020935149
19. EN 459-1: Building Lime – Part 1: Definitions, Specifications and Conformity Criteria. European Committee for Standardization (CEN), CEN/TC 51. Brussels, Belgium; 2015.
20. Giresini L, Sassu M, Sorrentino L. In situ free-vibration tests on unrestrained and restrained rocking masonry walls. *Earthquake Eng Struct Dyn*. 2018;47(15):3006-3025. https://doi.org/10.1002/eqe.3119
21. EN 1015-11: Methods of Test for Mortar for Masonry – Part 11: Determination of Flexural and Compressive Strength of Hardened Mortar. European Committee for Standardization (CEN), CEN/TC 125. Brussels, Belgium; 2007.
22. EN 772-1: Methods of Test for Masonry Units – Part 1: Determination of Compressive Strength. European Committee for Standardization (CEN), CEN/TC 125. Brussels, Belgium; 2011.
23. EN 1052-1: Methods of Test for Masonry – Part 1: Determination of Compressive Strength. European Committee for Standardization (CEN), CEN/TC 125. Brussels, Belgium; 2001.
24. EN 1052–5: Methods of Test for Masonry – Part 5: Determination of Bond Strength by the Bond Wrench Method. European Committee for Standardization (CEN), CEN/TC 125. Brussels, Belgium; 2005.
25. EN 1052–3: Methods of Test for Masonry – Part 3: Determination of Initial Shear Strength. European Committee for Standardization (CEN), CEN/TC 125. Brussels, Belgium; 2007.
26. Kallioras S, Grottoli L, Panatti M, Graziotti F, Shake-table experiments on three identical unreinforced clay-brick masonry buildings under uni-, bi-, and tri-directional seismic input motions. *EUCENTRE Research Report EUC64/2020U*, EUCENTRE, Pavia, Italy, 2020. Available at www.eucentre.it/nam-project
27. Kallioras S, Guerrini G, Tomassetti U, et al. Experimental seismic performance of a full-scale unreinforced clay-masonry building with flexible timber diaphragms. *Eng Struct*. 2018;161:231-249. https://doi.org/10.1016/j.engstruct.2018.02.016
28. Kallioras S, Correia AA, Graziotti F, Penna A, Magenes G. Collapse shake-table testing of a clay-URM building with chimneys. *Bull Earthquake Eng*. 2019;18(3):1009-1048. https://doi.org/10.1007/s10518-019-00730-0
29. Baker JW. Quantitative classification of near-fault ground motions using wavelet analysis. *Bull Seismol Soc Am*. 2007;97(5):1486-1501. https://doi.org/10.1785/0120060255
30. Den Bezemer T, Van Elk J, Special report on the Zeerijp Earthquake, January 8, 2018. *Research Report NAM, Nederlandse Aardolie Maatschappij*, Assen, The Netherlands, 2018. Available at www.nam.nl/feiten-en-cijfers (Accessed April 9, 2021).
31. Pinho R Personal communication in September 2019. The ground motion records from the Groningen gas field are available on the KNMI Data Centre platform at dataplatform.knmi.nl/ (Accessed April 9, 2021).

32. Amirbekian RV, Bolt BA. Spectral comparison of vertical and horizontal seismic strong ground motions in alluvial basins. *Earthquake Spectra*. 1998;14(4):573-595. https://doi.org/10.1193/1.1586017
33. Beresnev IA. Properties of vertical ground motions. *Bull Seismol Soc Am*. 2002;92(8):3152-3164. https://doi.org/10.1785/0120020009
34. Kruiver PP, van Dedem E, Romijn R, et al. An integrated shear-wave velocity model for the Groningen gas field, The Netherlands. *Bull Earthquake Eng*. 2017; 15(9):3555-3580. https://doi.org/10.1007/s10518-017-0105-y
35. Iervolino I, Baltzopoulos G, Chioccarelli E, Suzuki A. Seismic actions on structures in the near-source region of the 2016 central Italy sequence. *Bull Earthquake Eng*. 2017;17(10):5429-5447. https://doi.org/10.1007/s10518-017-0295-3
36. Zimmaro P, Scasserra G, Stewart JP, et al. Strong ground motion characteristics from 2016 Central Italy earthquake sequence. *Earthquake Spectra*. 2018;34(4):1611-1637. https://doi.org/10.1193/091817eqs184m
37. Özcebe AG, Lai C, Zuccolo E, Andreotti G, Personal communication on September 17, 2019. The ground motion records from the event of October 26 of the 2016 Central Italy earthquake sequence, and a power-point presentation of the selection procedure are available upon request at www.eucentre.it/nam-project
38. Pacor F, Felicetta C, Lanzano G, et al. NESS1: A worldwide collection of strong-motion data to investigate near-source effects. *Seismol Res Lett*. 2018;89(6):2299-2313. https://doi.org/10.1785/0220180149
39. Galadini F, Falcucci E, Gori S, Zimmaro P, Cheloni D, Stewart JP. Active faulting in source region of 2016–2017 Central Italy event sequence. *Earthquake Spectra*. 2018;34(4):1557-1583. https://doi.org/10.1193/101317eqs204m
40. Arias A. A measure of earthquake intensity. In: Hansen RJ, ed. *Seismic Design of Nuclear Power Plants*. Cambridge, Massachusetts, United States: MIT Press; 1970:438-483.
41. Eads L, Miranda E, Lignos DG. Average spectral acceleration as an intensity measure for collapse risk assessment. *Earthquake Eng Struct Dyn*. 2015;44(12):2057-2073. https://doi.org/10.1002/eqe.2575
42. Electrical Power Research Institute (EPRI). *A Criterion for Determining Exceedance of the Operating Basis Earthquake, EPRI Report NP-5930*. Electrical Power Research Institute: Palo Alto, California, United States; 1988.
43. Housner GW, Intensity of ground motion during strong earthquakes, *Caltech Technical Report*, California Institute of Technology, Pasadena, California, United States, 1952. Available at http://authors.library.caltech.edu (Accessed April 9, 2021).
44. Magenes G, Penna A, Senaldi IE, Rota M, Galasco A. Shaking table test of a strengthened full-scale stone masonry building with flexible diaphragms. *Int J Architect Heritage*. 2013;8(3):349-375. https://doi.org/10.1080/15583058.2013.826299
45. Graziotti F, Penna A, Magenes G. A nonlinear SDOF model for the simplified evaluation of the displacement demand of low-rise URM buildings. *Bull Earthquake Eng*. 2016;14(6):1589-1612. https://doi.org/10.1007/s10518-016-9896-5
46. Kallioras S, Graziotti F, Penna A. Numerical assessment of the dynamic response of a URM terraced house exposed to induced seismicity. *Bull Earthquake Eng*. 2018;17(3):1521-1552. https://doi.org/10.1007/s10518-018-0495-5
47. Bommer JJ, Martínez-Pereira A. The effective duration of earthquake strong motion. *J Earthquake Eng*. 1999;3(2):127-172. https://doi.org/10.1080/13632469909350343
48. Kempton JJ, Stewart JP. Prediction equations for significant duration of earthquake ground motions considering site and near-source effects. *Earthquake Spectra*. 2006;22(4):985-1013. https://doi.org/10.1193/1.2358175
49. Bradley BA. Correlation of Arias intensity with amplitude, duration and cumulative intensity measures. *Soil Dyn Earthquake Eng*. 2015;78:89-98. https://doi.org/10.1016/j.soildyn.2015.07.009
50. Travasarou T, Bray JD, Abrahamson NA. Empirical attenuation relationship for Arias Intensity. *Earthquake Eng Struct Dyn*. 2003;32(7):1133-1155. https://doi.org/10.1002/eqe.270
51. Costley AC, Abrams DP, Dynamic response of unreinforced masonry buildings with flexible diaphragms. *Technical Report, Structural Research Series No. 605*, University of Illinois at Urbana-Champaign, Urbana, Illinois, United States, 1995. Available at http://hdl.handle.net/2142/14227 (Accessed April 9, 2021).
52. Makris N, Konstantinidis D. The rocking spectrum and the limitations of practical design methodologies. *Earthquake Eng Struct Dyn*. 2002;32(2):265-289. https://doi.org/10.1002/eqe.223
53. Vassiliou MF, Mackie KR, Stojadinović B. Dynamic response analysis of solitary flexible rocking bodies: Modeling and behavior under pulse-like ground excitation. *Earthquake Eng Struct Dyn*. 2014;43(10):1463-1481. https://doi.org/10.1002/eqe.2406
54. Elgamal A, He L. Vertical earthquake ground motion records: An overview. *J Earthquake Eng*. 2004;8(5):663-697. https://doi.org/10.1080/13632460409350505

How to cite this article: Kallioras S, Graziotti F, Penna A, Magenes G. Effects of vertical ground motions on the dynamic response of URM structures: Comparative shake-table tests. *Earthquake Engng Struct Dyn*. 2022;51:347–368. https://doi.org/10.1002/eqe.3569